THREE DIMENSIONAL FINITE STRAIN ROD MODEL – PART II: COMPUTATIONAL ASPECTS

by

J. C. Simo and L. Vu Quoc

Memorandum No. UCB/ERL M85/31

23 April 1985

COVER

THREE DIMENSIONAL FINITE STRAIN ROD MODEL

PART II: COMPUTATIONAL ASPECTS

by

J. C. Simo and L. Vu Quoc

Memorandum No. UCB/ERL M85/31

23 April 1985

ELECTRONICS RESEARCH LABORATORY

College of Engineering
University of California, Berkeley
94720

Three Dimensional Finite Strain Rod Model. Part II: Computational Aspects.

J.C. SIMO and L. VU QUOC

University of California, Berkeley, CA 94720.

Abstract

The variational formulation and computational aspects of a three dimensional finite strain rod model considered in Simo [1985] are presented. A particular parametrization is employed that by-passes the singularity typically associated with the use of Euler angles. As in the classical Kirchhoff-Love model, rotations have the standard interpretation of orthogonal, generally non-commutative, transformations. This is in contrast with alternative formulations proposed by Argyris et.al [1979,1981,1982], based on the notion of semi-tangential rotation. Emphasis is placed on a geometric approach which proves essential in the formulation of algorithms. In particular, the configuration update procedure becomes the algorithmic counterpart of the *exponential map*. The computational implementation relies on the formula for the exponential of a skew-symmetric matrix. Consistent linearization procedures are employed to obtain linearized weak forms of the balance equations. The *geometric stiffness* then becomes generally *non-symmetric* as a result of the non-Euclidean character of the configuration space. However, complete *symmetry* is recovered at an *equilibrium* configuration, provided that the loading is conservative. An explicit condition for this to be the case is obtained. Numerical simulations including post-buckling behavior and non-conservative loading are also presented. Details pertaining to the implementation of the present formulation are also discussed.

Contents

April 22, 1985

1. Introduction.

This paper is concerned with the variational formulation and numerical implementation in the context of the finite element method of the three dimensional finite strain rod model considered in Simo [1985]. We recall that this model is essentially a re-parametrization of an extension to the classical Kirchhoff-Love model, developed by Antman [1974,1975] in the context of a director approach, which includes finite extension and shearing of the rod. The parametrization employed here, however, avoids the use of Euler angles and its associated singularity, and plays a basic role in the computational implementation. In the context of aircraft dynamics, issues concerning alternative parametrizations are addressed in e.g., de Veubeke [1976] and Kane [1983].

A basic feature of the present approach concerns the treatment of the rotation field of the rod. In the present model, as in the classical Kirchoff-Love model, rotations have the traditional meaning of orthogonal transformations in Euclidean space. We recall that orthogonal transformations constitute a *non-commutative* (Lie) group referred to as the special orthogonal group, SO(3). This approach is in contrast with that proposed by Argyris and co-workers [1979,1981,1982] in which the standard notion of rotation is replaced by the so-called *semi-tangential* rotation. Thus, for the present rod model the configuration space is no longer linear, but becomes a differentiable manifold. The dynamical description of the heavy top furnishes another familiar example of dynamical system whose configuration space, SO(3), is a (nonlinear) manifold (e.g. Marsden, Ratiu & Wenstein [1984]). This example is in fact closely related to the Kirchhoff-Love model through the so-called kinetic analogy (Love [1944]).

The finite element procedure developed in this paper is based on a variational formulation, discussed in Section 4, of a precisely stated set of partial differential equations summarized in Section 2. We emphasize that these equations reduce to the classical Kirchhoff-Love model for vanishing shearing and small axial strains. For this model, a numerical treatment restricted to circular cross sections and particular loading is considered in Nordgren [1974]. Consistent linearization procedures, Marsden & Hughes [1983], are employed to obtain the linearized weak form of momentum balance. The resulting *global* tangent operator is characterized by possessing a *non-symmetric geometric stiffness*. This lack of symmetry arises from the non-commutativity of the special rotation group, SO(3). Argyris et. al. [1982] pointed out that this lack of symmetry inevitably arises at the element (*local*) level, although it is stated that symmetry is recovered upon assembly at the *global* level (Argyris et. al. [1982, pag. 2]). Such a result is attributed by these authors to a deficiency of the classical definitions of moment and rotation, and motivated to a large extent their adoption of a numerical formulation entirely based on the concept of semi-tangential rotation introduced by Ziegler [1977]. On the other hand, in the context of a classical formulation of rotations, it is shown in Section 5 that

(i) The *global geometric stiffness* arising for the (consistently) linearized weak form is *non symmetric*, even for conservative loading, at a *non-equilibrium* configuration.

(ii) At an *equilibrium* configuration the linearized tangent operator is *always symmetric* provided the loading is conservative. A condition for this then follows, with a structure similar to that discussed by Schweizerhof and Ramm [1984] and Bufler [1984] for pressure loading.

(iii) Upon discretization, from (ii) it follows that both the global and the local (element) geometric stiffness matrices are *symmetric* at an *equilibrium* configuration.

Emphasis is placed throughout the formulation on a geometric approach that enables one to formulate efficient algorithms. A configuration of the rod is described by a vector field giving the position of the current line of centroids and an orthogonal "moving" frame which physically models the cross section. The moving frame is positioned by an orthogonal matrix, and the vorticity of the frame becomes the rotational degree of freedom. The configuration update procedure then becomes the algorithmic counterpart of the so-called exponential map. Conceptually, for the problem at hand the procedure amounts to the following: for fixed $S \in [0, L]$, the incremental (*infinitesimal*) rotation, defined by a skew-symmetric matrix, is first "exponentiated" to obtain a finite rotation defined by an orthogonal matrix. This matrix is then multiplied by the existing rotation (another orthogonal matrix) to complete the update. This procedure relies crucially on the closed form formula for the exponential of a skew-symmetric matrix.‡ This formula, referred to as Rodrigues' formula in the sequel, enables one to evaluate *exactly* the exponential of a (possibly non-constant) skew-symmetric matrix. In addition, by making use of Rodrigues' formula, it is possible to obtain a simple *closed form* expression for the derivative of the exponential map, which plays a crucial role in the evaluation of the curvatures of the rod. A detailed discussion of the finite element formulation and the configuration update procedure is presented in Section 6.

From a computational standpoint, an implementation based on the use of quaternion parameters proves to be the optimal choice that avoids singularity and minimizes storage requirements. The relevant practical aspects of this implementation are discussed in detail in Appendix II.

The formulation discussed in this paper is illustrated in Section 7 through a set of numerical simulation including plane and three dimensional problems, and both conservative and non-conservative loading. An effort has been made to compare the results with those in the existing literature, as in Argyris [1981,1982], and Bathe [1979].

2. Finite strain beam model. Summary.

In this section we summarize the basic features of the rod model employed in this paper. We recall that this model is essentially equivalent to that developed by Antman [1974] in the context of a director type of formulation, as an extension of the classical Kirchhoff-Love rod model, Love [1944]. This extension accounts for finite extension and shearing of the rod. The two dimensional version of this model is due to Reissner [1972].

Kinematic description. (See Fig. 2.1) Let $\{\mathbf{t}_I(S,t)\}_{\{I=1,2,3\}}$ represent the orthonormal basis vector of a moving frame attached to a typical cross-section, where $S \in [0,L] \subset \mathbb{R}$ denotes the (curvilinear) coordinate along the line of centroids of the undeformed beam, and $t \in \mathbb{R}_+$ is a time parameter. The origin of the moving frame is fixed at the centroid of the cross-section, and $\mathbf{t}_3(S)$ remains normal to the section at all times. The *fixed* reference (*material*) basis of the same section is denoted by $\{\mathbf{E}_I(S)\}_{\{I=1,2,3\}}$, so that $\{\mathbf{t}_I(S,0)\}_{\{I=1,2,3\}} = \{\mathbf{E}_I(S)\}_{\{I=1,2,3\}}$, for $S \in [0,L]$. The *fixed* spatial basis is denoted by $\{\mathbf{e}_i\}_{\{i=1,2,3\}}$. In what follows, for simplicity we assume $\mathbf{E}_I$ constant, so that spatial and material basis may be taken as coincident, i.e., $\mathbf{e}_k = \mathbf{E}_k$, for $k=1,2,3$. The *orientation* of the *moving* frame $\{\mathbf{t}_I(S,t)\}_{\{I=1,2,3\}}$ along $S \in [0,L]$, and through time $t \in \mathbb{R}_+$, is specified by an *orthogonal* transformation $\mathbf{\Lambda}(S,t) = \Lambda_{iJ}(S,t)\, \mathbf{e}_i \otimes \mathbf{E}_J$ † such that

‡ This formula is closely related to the one often ascribed to Rodrigues. See, e.g., the footnote on pag. 165 of Goldstein [1981], Argyris [1982], and Kane et. al. [1983].

† Summation convention on repeated indices is implied, and $\otimes$ denotes standard tensor pro-

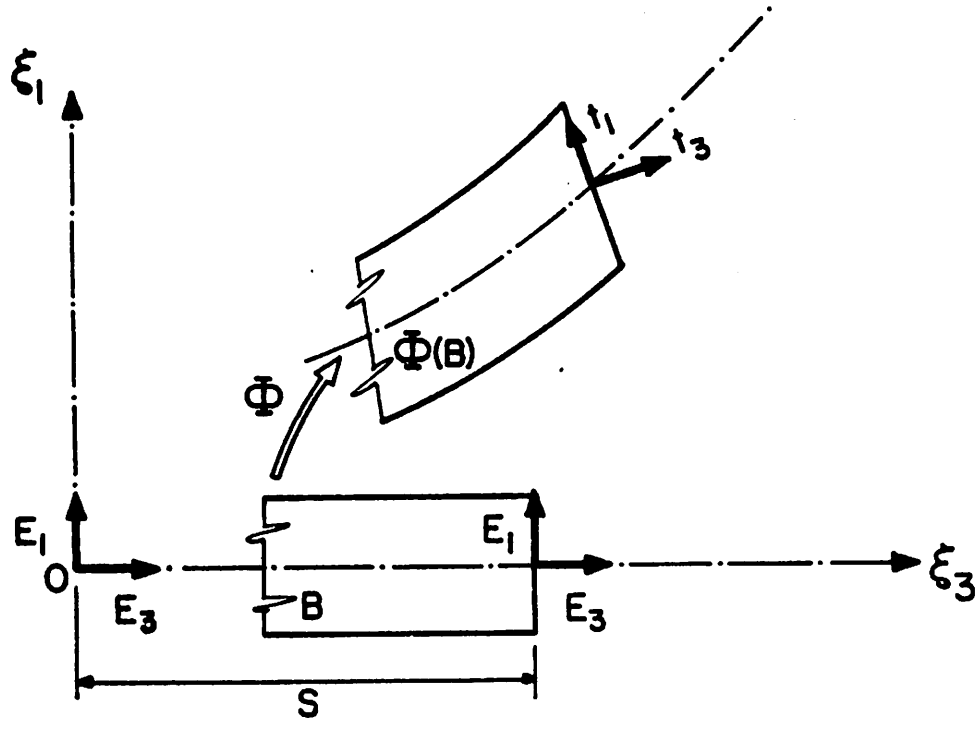

Fig. 2.1. Kinematic description of the rod for the plane problem. Definition of various frames.

$$\mathbf{t}_I(S,t) = \mathbf{\Lambda}(S,t)\mathbf{E}_I = \Lambda_{iI}(S,t)\,\mathbf{e}_i\,, \quad (I=1,2,3)\,. \tag{2.1a}$$

The position $\mathbf{x}_0 \in \mathbb{R}^3$ of the centroid of the cross section (i.e., the origin of the moving frame) is defined by the curve

$$\mathbf{x}_0 = \boldsymbol{\phi}_0(S,t) = \phi_{0i}(S,t)\,\mathbf{e}_i\,. \tag{2.1b}$$

Accordingly, the set C of all possible configurations of the rod is defined by

$$C \triangleq \{\, \boldsymbol{\phi} \equiv (\boldsymbol{\phi}_0, \mathbf{\Lambda}) \;\big|\; \boldsymbol{\phi}_0 : (0,L) \to \mathbb{R}^3,\ \mathbf{\Lambda} : (0,L) \to SO(3) \,\} \tag{2.1c}$$

Here, $SO(3)$ is the special orthogonal (Lie) group. See Fig. 2.1. The alternative expressions in the *spatial* and *material* descriptions, of the derivatives of the *orthogonal* transformation $(S,t) \to \mathbf{\Lambda}(S,t)$ are summarized Box 1.

---

duct.

BOX 1. *Derivatives of moving frame*

Spatial	Material
$\dfrac{\partial \Lambda(S,t)}{\partial S} = \Omega(S,t)\,\Lambda(S,t)$	$\dfrac{\partial \Lambda(S,t)}{\partial S} = \Lambda(S,t)\,K(S,t)$
$\Omega \triangleq \begin{bmatrix} 0 & -\omega_3 & \omega_2 \\ \omega_3 & 0 & -\omega_1 \\ -\omega_2 & \omega_1 & 0 \end{bmatrix}$	$K \triangleq \begin{bmatrix} 0 & -\kappa_3 & \kappa_2 \\ \kappa_3 & 0 & -\kappa_1 \\ -\kappa_2 & \kappa_1 & 0 \end{bmatrix}$
$\boldsymbol{\omega} \triangleq \omega_1 \mathbf{e}_1 + \omega_2 \mathbf{e}_2 + \omega_3 \mathbf{e}_3$ $= \kappa_1 \mathbf{t}_1 + \kappa_2 \mathbf{t}_2 + \kappa_3 \mathbf{t}_3$	$K \triangleq \kappa_1 \mathbf{E}_1 + \kappa_2 \mathbf{E}_2 + \kappa_3 \mathbf{E}_3$
$\dfrac{\partial \Lambda(S,t)}{\partial t} = \mathbb{W}(S,t)\,\Lambda(S,t)$	$\dfrac{\partial \Lambda(S,t)}{\partial t} = \Lambda(S,t)\,\overline{\mathbb{W}}(S,t)$
$\mathbf{w} \triangleq w_1 \mathbf{e}_1 + w_2 \mathbf{e}_2 + w_3 \mathbf{e}_3$ $= \overline{w}_1 \mathbf{t}_1 + \overline{w}_2 \mathbf{t}_2 + \overline{w}_2 \mathbf{t}_3$	$\overline{\mathbf{w}} \triangleq \overline{w}_1 \mathbf{E}_1 + \overline{w}_2 \mathbf{E}_2 + \overline{w}_3 \mathbf{E}_3$

Note that $\mathbf{\Lambda}\mathbf{\Lambda}^T = 1$ and that $K + K^T = 0$, $\Omega + \Omega^T = 0$. Similarly, $\mathbb{W} + \mathbb{W}^T = 0$, and $\overline{\mathbb{W}} + \overline{\mathbb{W}}^T = 0$.

Stress resultants and couples. Conjugate strain measures. Denoting by $\mathbf{P} \equiv \sum_{I=1,3} \mathbf{T}_I \otimes \mathbf{E}_I$ the non-symmetric (first) Piola-Kirchhoff stress tensor, the stress resultant, $\mathbf{n} = n_i\,\mathbf{e}_i$, and the *spatial* stress couple, $\mathbf{m} = m_i\,\mathbf{e}_i$, over a cross section $\Gamma \subset \mathbb{R}^2$ in its *current* configuration, are defined as

$$\mathbf{n} \triangleq \int_\Gamma \mathbf{T}_3\, d\Gamma\,; \quad \mathbf{m} \triangleq \int_\Gamma [\mathbf{x} - \boldsymbol{\phi}_0(S,t)] \times \mathbf{T}_3\, d\Gamma \tag{2.2}$$

The *material* stress resultant, $\mathbf{N} = N_I\,\mathbf{E}_I$ and stress couple, $\mathbf{M} = M_I\,\mathbf{E}_I$, are obtained by transforming $\mathbf{n}$ and $\mathbf{m}$ to the reference configuration (*pull-back*); i.e.,

$$\mathbf{n}(S,t) = \mathbf{\Lambda}(S,t)\,\mathbf{N}(S), \qquad \mathbf{m}(S,t) = \mathbf{\Lambda}(S,t)\,\mathbf{M}(S). \tag{2.3}$$

Note that the components of $\mathbf{n}$ and $\mathbf{m}$ in the moving frame $\{\mathbf{t}_I\}$ are identically the same as the components in the basis $\{\mathbf{E}_I\}$ of $\mathbf{N}$ and $\mathbf{M}$, respectively; i.e., $\mathbf{n} = N_I\,\mathbf{t}_I$ and $\mathbf{m} = M_I\,\mathbf{t}_I$. Similarly, the components of $\boldsymbol{\omega}$ in the moving frame equal those of K in the material frame, as shown in Box 1.

Appropriate *strain* measures *conjugate* to the corresponding stress resultant and stress couple are obtained through the *stress power* equivalence

$$\int_{\Gamma\times[0,L]} \mathbf{P} : \dot{\mathbf{F}}\, d\Gamma dS = \int_{[0,L]} [\mathbf{n} \cdot \overset{\nabla}{\boldsymbol{\gamma}} + \mathbf{m} \cdot \overset{\nabla}{\boldsymbol{\omega}}]\, dS = \int_{[0,L]} [\mathbf{N} \cdot \dot{\mathbf{\Gamma}} + \mathbf{M} \cdot \dot{K}]\, dS \tag{2.4}$$

where $\mathbf{F}$ is the deformation gradient, and a superposed "dot" denotes time differentiation. Here, $\overset{\nabla}{(\cdot)} \triangleq \dfrac{\partial}{\partial t}(\cdot) - \mathbf{w} \times (\cdot)$ denotes the *co-rotated* rate; that is, the rate measured by an observer attached to the moving frame. The expressions of the spatial and material conjugate strains are summarized in Box 2. below.

BOX 2. *Strain measures*

spatial	material
$\boldsymbol{\gamma} = \dfrac{\partial \boldsymbol{\phi}_0(S,t)}{\partial S} - \mathbf{t}_3$	$\boldsymbol{\Gamma} = \boldsymbol{\Lambda}^T \dfrac{\partial \boldsymbol{\phi}_0(S,t)}{\partial S} - \mathbf{E}_3$
$\boldsymbol{\omega}$	$\boldsymbol{K} = \boldsymbol{\Lambda}^T \boldsymbol{\omega}$

Remark 2.1. The following relation between the *spatial* and *material* strain rates should be noted

$$\overset{\nabla}{\boldsymbol{\gamma}} = \boldsymbol{\Lambda} \frac{\partial}{\partial t} \boldsymbol{\Lambda}^T \boldsymbol{\gamma} \equiv \boldsymbol{\Lambda} \dot{\boldsymbol{\Gamma}}, \qquad \overset{\nabla}{\boldsymbol{\omega}} = \boldsymbol{\Lambda} \frac{\partial}{\partial t} \boldsymbol{\Lambda}^T \boldsymbol{\omega} \equiv \boldsymbol{\Lambda} \dot{\boldsymbol{K}} \tag{2.5}$$

These relations show that $\overset{\nabla}{(\cdot)}$ is a particular form of Lie derivative in which pull-back/ push-forward operations are performed with $\boldsymbol{\Lambda}$. See, Marsden & Hughes [1983, Sec.1.7] ▪

Balance laws and constitutive equations. Local form. We summarize below the system of partial differential equations to be solved, consisting of the balance laws and constitutive equations expressed in local form. The *spatial* form of the local balance laws is given by

$$\frac{\partial}{\partial S}\mathbf{n} + \bar{\mathbf{n}} = \rho A \ddot{\boldsymbol{\varphi}}_o, \tag{2.6a}$$

$$\frac{\partial}{\partial S}\mathbf{m} + \frac{\partial \boldsymbol{\phi}_0}{\partial S} \times \mathbf{n} + \bar{\mathbf{m}} = \rho \mathbf{I}\dot{\mathbf{w}} + \mathbf{w} \times [\rho \mathbf{I}\mathbf{w}], \tag{2.6b}$$

where A and $\mathbf{I}$ denote the area and inertia tensor of a cross section at $S \in (0,L)$, and $\rho = \rho(S)$ is the mass density (per unit of reference length). In addition, constitutive equations expressed in the *spatial* descriptions take the form

$$\mathbf{n} = \frac{\partial \psi(S,\boldsymbol{\gamma},\boldsymbol{\omega})}{\partial \boldsymbol{\gamma}}, \quad \text{and} \quad \mathbf{m} = \frac{\partial \psi(S,\boldsymbol{\gamma},\boldsymbol{\omega})}{\partial \boldsymbol{\omega}}. \tag{2.7}$$

Alternatively, in the *material* description one has the expressions

$$\mathbf{N} = \frac{\partial \Psi(S,\boldsymbol{\Gamma},\boldsymbol{K})}{\partial \boldsymbol{\Gamma}}, \quad \text{and} \quad \mathbf{M} = \frac{\partial \Psi(S,\boldsymbol{\Gamma},\boldsymbol{K})}{\partial \boldsymbol{K}}. \tag{2.8}$$

The functions ψ and Ψ are subjected to the invariance requirements under superposed rigid body motions, Naghdi [1972], Antman [1972]. Finally, one defines the *material* elasticity tensor according to the expression

$$\mathbf{C}(S,\boldsymbol{\Gamma},\boldsymbol{K}) \equiv \begin{bmatrix} \dfrac{\partial \Psi}{\partial \boldsymbol{\Gamma} \partial \boldsymbol{\Gamma}} & \dfrac{\partial \Psi}{\partial \boldsymbol{\Gamma} \partial \boldsymbol{K}} \\ \dfrac{\partial \Psi}{\partial \boldsymbol{\Gamma} \partial \boldsymbol{K}} & \dfrac{\partial \Psi}{\partial \boldsymbol{K} \partial \boldsymbol{K}} \end{bmatrix} \tag{2.9}$$

The *spatial* form of the elasticity tensor can be also defined. In the development that follows, $\mathbf{C}$ is often assumed constant and diagonal; hence given by

$$\mathbf{C} = Diag\,[GA_1, GA_2, EA, EI_1, EI_2, GJ] \tag{2.10}$$

Here, GA_1 and GA_2 denote the shear stiffness along $\mathbf{t}_1$ and $\mathbf{t}_2$, EA is the axial stiffness, EI_1 and EI_2 are the principal bending stiffnesses relative to $\mathbf{t}_1$ and $\mathbf{t}_2$, and GJ is the torsional stiffness of the rod.

This completes our summary of the rod model considered in this paper. The numerical treatment to be developed hinges on the the variational form of the equations summarized above, and considered in Section 4.

3. Admissible variations. Consistent linearization.

A distinct characteristic of the model problem summarized above is that the configuration space C is a *differentiable manifold* and not a linear space, due to presence of the special orthogonal group (SO(3)) in the definition of C. In this section we first consider the appropriate definition of *admissible variations* which play an essential role in the variational formulation of the governing equations. The consistent linearization of the strain measures summarized in Box 2 about an arbitrary configuration is considered next. These results are essential for the linearization of the variational equations addressed in Section 4.

3.1. Admissible variations.

Consider an arbitrary configuration of the rod specified by the position of its line of centroids and the orientation of the moving frame; that is

$$\boldsymbol{\phi}(S) \equiv (\boldsymbol{\phi}_0(S), \boldsymbol{\Lambda}(S)) \in C \tag{3.1}$$

We construct a perturbed (or varied) configuration relative to $\boldsymbol{\phi}(S)$, denoted by $\boldsymbol{\phi}_\varepsilon(S)$ as follows. Let $\boldsymbol{\eta}_0(S) = \eta_{0i}\,\mathbf{e}_i$ be a vector field interpreted, for $\varepsilon > 0$, as a *superposed infinitesimal displacement* onto the line of centroids defined by $\boldsymbol{\phi}_0(S)$. In addition, let $\boldsymbol{\Theta}(S)$ be a *skew-symmetric* tensor field interpreted, for $\varepsilon > 0$, as a *superposed infinitesimal rotation* onto the moving frame defined by $\boldsymbol{\Lambda}(S)$, with an axial vector $\varepsilon\,\boldsymbol{\vartheta}(S)$. In components we have

$$\boldsymbol{\eta}_0(S) = \eta_{0i}\,\mathbf{e}_i\,, \qquad \boldsymbol{\Theta}(S) = \Theta_{ij}(S)\,\mathbf{e}_i \otimes \mathbf{e}_j \tag{3.2}$$

The *"perturbed"* configuration $\boldsymbol{\phi}_\varepsilon(S) \equiv (\boldsymbol{\phi}_{0\varepsilon}(S), \boldsymbol{\Lambda}_\varepsilon(S)) \in C$ is then obtained by setting

$$\boldsymbol{\phi}_{0\varepsilon}(S) = \boldsymbol{\phi}_0(S) + \varepsilon\,\boldsymbol{\eta}_0(S), \qquad \boldsymbol{\Lambda}_\varepsilon(S) = \exp[\varepsilon\,\boldsymbol{\Theta}(S)]\boldsymbol{\Lambda}(S) \tag{3.3}$$

It should be recalled that *finite rotations* are defined by *orthogonal* transformations, whereas *infinitesimal* rotations are obtained through *skew-symmetric* transformations. By *exponentiation* of a skew-symmetric matrix (infinitesimal rotation) one obtains an orthogonal matrix (finite rotation). Thus, $(3.3)_2$ is constructed so that $\boldsymbol{\Lambda}_\varepsilon$ *remains orthogonal* and thus defines a possible orientation of the moving frame. Hence, by construction, $\boldsymbol{\phi}_\varepsilon \in C$, for all $\varepsilon \in \mathbb{R}$.

Let us denote by $so(3)$ the (Lie) algebra of all *skew-symmetric* tensors. Given a skew-symmetric tensor, $\boldsymbol{\Theta} \in so(3)$, it is often more convenient to work with the associated *axial vector*, denoted by $\boldsymbol{\vartheta} \in \mathbb{R}^3$, and defined so that

$$\boldsymbol{\Theta}\,\mathbf{h} = \boldsymbol{\vartheta} \times \mathbf{h}, \qquad \text{for any } \mathbf{h} \in \mathbb{R}^3 \tag{3.4}$$

We note that $\boldsymbol{\omega}$ and $\boldsymbol{K}$ in Box 1 are simply the axial vectors of $\boldsymbol{\Omega}$ and K, respectively. Similarly, $\mathbf{w}$ is the axial vector (angular velocity) associated with $\mathbf{W}$. Henceforth, a pair $\boldsymbol{\eta}(S) \equiv (\boldsymbol{\eta}_0(S), \boldsymbol{\vartheta}(S)) \in \mathbb{R}^3 \times \mathbb{R}^3$ will be referred to as an *admissible variation*. The first argument, $\boldsymbol{\eta}_0(S)$, is interpreted as an *infinitesimal displacement* of the line of centroids, and the second argument $\boldsymbol{\vartheta}(S)$, is interpreted as a *superposed infinitesimal rotation* onto the moving frame.

For simplicity, in what follows attention is focused on the boundary value problem in which displacements and rotations are the prescribed boundary

data. Accordingly, the set of kinematically admissible variations (at the identity), denoted by $T_\phi C$ in the sequel, is given by

$$T_\phi C \equiv \{\eta(S) \equiv (\eta_0(S), \vartheta(S)) \in \mathbb{R}^3 \times \mathbb{R}^3 \mid \eta_0\big|_{S\in\{0,L\}} \equiv \vartheta\big|_{S\in\{0,L\}} = 0\} \quad (3.5)$$

In geometric terms one says that $T_\phi C$ † is the tangent space at the identity of the configuration space C.

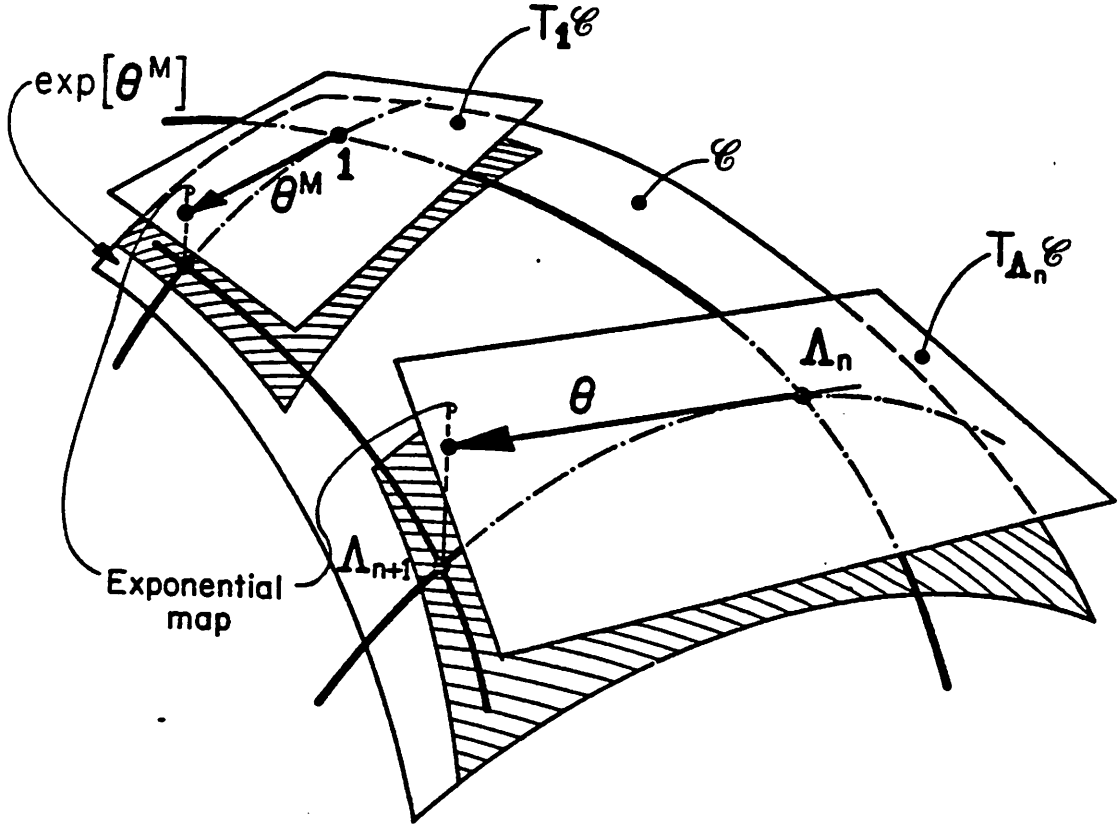

Fig. 3.1. Geometric interpretation of the exponential map.

Remark 3.1. Within the geometric context outlined in this section, $\Theta = \Theta_{ij}\, \mathbf{e}_i \otimes \mathbf{e}_j$ corresponds to a *spatial* infinitesimal rotation defined on the tangent space $T_\phi C$. Alternatively, one may consider the *material* counterpart Θ^M defined as

$$\Theta^M \triangleq \Lambda^T \Theta \Lambda, \quad \text{where} \quad \Theta^M \equiv \Theta^M_{IJ}\, \mathbf{E}_I \otimes \mathbf{E}_J \quad (3.6)$$

Upon recalling the property of the exponential map in $SO(3)$ that

† Strictly speaking, elements of the tangent space $T_\phi C$ at $\phi \equiv (\phi_0, \Lambda)$ are of the form $(\eta_0, \Theta\Lambda)$. See eq. (3.9) where the tangent to a curve of configurations is explicitly computed. Due to the one-to-one correspondence between $\mathbb{R}^3$ and $so(3)$, Θ may be replaced by its axial vector ϑ. In addition, with a slight abuse in notation, Λ will be often omitted. This justifies the notation employed in (3.5).

$$\mathbf{\Lambda}^T \exp[\boldsymbol{\Theta}]\mathbf{\Lambda} = \exp[\mathbf{\Lambda}^T \boldsymbol{\Theta} \mathbf{\Lambda}] \tag{3.7}$$

where $\mathbf{\Lambda} \in SO(3)$ and $\boldsymbol{\Theta} \in so(3)$, it follows that $(3.3)_2$ may be expressed in the equivalent forms

$$\mathbf{\Lambda}_\varepsilon = \exp[\varepsilon \boldsymbol{\Theta}]\mathbf{\Lambda} \equiv \mathbf{\Lambda} \exp[\varepsilon \boldsymbol{\Theta}^M] \tag{3.8}$$

The geometric interpretation of these relations is contained in Fig. 3.1, and leads to a simple update procedure discussed in Section 5.2. Geometrically, $\boldsymbol{\Theta}$ defines an (incremental) tangent field onto the current configuration given by $\mathbf{\Lambda}_n$. A subsequent configuration is obtained by means of the exponential map simply by setting $\mathbf{\Lambda}_{n+1} = \exp[\boldsymbol{\Theta}]\mathbf{\Lambda}_n$. Note that $\boldsymbol{\Theta}^M \in T_{identity} C$; that is, an infinitesimal rotation superposed onto the reference configuration. Thus, an equivalent update procedure is furnished by $\mathbf{\Lambda}_{n+1} = \mathbf{\Lambda}_n \exp[\boldsymbol{\Theta}^M]$. See Fig. 3.1. ▪

3.2. Linearization of strain measures.

Here, we consider the linearization of the strain measures summarized in Box 2. The basic set-up is as above: Given a configuration $\boldsymbol{\phi} \equiv (\boldsymbol{\phi}_0, \mathbf{\Lambda}) \in C$ we consider an admissible variation $\boldsymbol{\eta} \equiv (\boldsymbol{\eta}_0, \boldsymbol{\vartheta}) \in T_{\boldsymbol{\phi}} C$ and the corresponding superposed configuration $\boldsymbol{\phi}_\varepsilon \in C$ defined by (3.3). To systematically carry out the linearization process, we make use of the notion of *directional derivative*. First, we note that for the superposed configuration defined by (3.3), by taking the directional derivative one has

$$\begin{aligned} D\boldsymbol{\phi}_0 \cdot \boldsymbol{\eta}_0 &\triangleq \left. \frac{d}{d\varepsilon} \right|_{\varepsilon=0} \boldsymbol{\phi}_{0\varepsilon}(S) = \boldsymbol{\eta}_0(S) \\ D\mathbf{\Lambda} \cdot \boldsymbol{\Theta} &\triangleq \left. \frac{d}{d\varepsilon} \right|_{\varepsilon=0} \mathbf{\Lambda}_\varepsilon(S) = \boldsymbol{\Theta}(S)\, \mathbf{\Lambda}(S) \end{aligned} \tag{3.9}$$

Next, we proceed to linearize the strain measures in Box 2 about the configuration $\boldsymbol{\phi} \in C$.

Linearization of $\boldsymbol{\Omega}$ *and* $\mathbf{K}$. Making use of the definition of $\boldsymbol{\Omega}$ in Box 1, we have

$$\boldsymbol{\Omega}_\varepsilon \equiv \frac{d\mathbf{\Lambda}_\varepsilon}{dS} \mathbf{\Lambda}_\varepsilon^T = \left(\frac{d \exp[\varepsilon \boldsymbol{\Theta}]}{dS}\right) \exp[-\varepsilon \boldsymbol{\Theta}] + \exp[\varepsilon \boldsymbol{\Theta}]\, \boldsymbol{\Omega} \exp[-\varepsilon \boldsymbol{\Theta}] \tag{3.10}$$

To proceed further, one needs to compute the derivative of the exponential of a skew-symmetric matrix. This is done in Appendix I and relies crucially on the following formula, which is closely related to Rodrigues' formula (Goldstein [1981], Argyris [1982], Kane [1983])

$$\exp[\boldsymbol{\Theta}(S)] = \mathbf{I} + \frac{2}{1 + \|\bar{\boldsymbol{\vartheta}}\|^2} (\bar{\boldsymbol{\Theta}} + \bar{\boldsymbol{\Theta}}^2) \tag{3.11a}$$

Here, $\bar{\boldsymbol{\vartheta}}(S)$ is the axial vector of $\bar{\boldsymbol{\Theta}}(S)$, and is the so-called pseudo-vector of rotation (see Appendix II). $\bar{\boldsymbol{\vartheta}}(S)$ is related to the axial vector $\boldsymbol{\vartheta}(S)$ of $\boldsymbol{\Theta}(S)$ according to the expression

$$\bar{\boldsymbol{\vartheta}} = \tfrac{1}{2} \frac{\tan(\|\boldsymbol{\vartheta}\|/2)}{\|\boldsymbol{\vartheta}\|/2} \boldsymbol{\vartheta} \tag{3.11b}$$

The expression for the derivative of the exponential of a skew-symmetric tensor then takes the form

$$\left(\frac{d \exp[\boldsymbol{\Theta}]}{dS}\right) \exp[-\boldsymbol{\Theta}] = \frac{2}{1 + \|\bar{\boldsymbol{\vartheta}}\|^2} (\bar{\boldsymbol{\Theta}}' + \bar{\boldsymbol{\Theta}}' \bar{\boldsymbol{\Theta}} - \bar{\boldsymbol{\Theta}} \bar{\boldsymbol{\Theta}}') \tag{3.11c}$$

where $\bar{\boldsymbol{\Theta}}' \triangleq d\bar{\boldsymbol{\Theta}}/dS$. By replacing $\boldsymbol{\Theta}(S)$ by $\varepsilon\boldsymbol{\Theta}(S)$ in (3.11b) and (3.11c), taking the derivative relative to ε and particularizing at $\varepsilon = 0$, it follows that

$$\frac{d}{d\varepsilon}\Big|_{\varepsilon=0} \left(\frac{d\exp[\varepsilon\boldsymbol{\Theta}]}{dS}\right)\exp[-\varepsilon\boldsymbol{\Theta}] = \boldsymbol{\Theta}' \tag{3.12}$$

Therefore, with the aid of (3.12), the directional derivative of (3.10) may be expressed as

$$D\boldsymbol{\Omega}\cdot\boldsymbol{\Theta} \equiv \frac{d}{d\varepsilon}\Big|_{\varepsilon=0} \boldsymbol{\Omega}_\varepsilon = \boldsymbol{\Theta}' + \boldsymbol{\Theta}\boldsymbol{\Omega} - \boldsymbol{\Omega}\boldsymbol{\Theta} \tag{3.13}$$

Similarly, since $\boldsymbol{K}_\varepsilon = \boldsymbol{\Lambda}_\varepsilon^T \dfrac{\partial \boldsymbol{\Lambda}_\varepsilon}{\partial S}$, an analogous calculation shows that

$$D\boldsymbol{K}\cdot\boldsymbol{\Theta} \triangleq \frac{d}{d\varepsilon}\Big|_{\varepsilon=0} \boldsymbol{K}_\varepsilon = \boldsymbol{\Lambda}^T\boldsymbol{\Theta}'\boldsymbol{\Lambda} \tag{3.14}$$

Linearization of $\boldsymbol{\omega}$ and $\boldsymbol{K}$. In order to obtain the linearization of $\boldsymbol{\omega}(S)$ one simply needs to express (3.13) in terms of axial vectors. For this purpose, recall that the commutator (Lie bracket) of two skew-symmetric matrices may be expressed as

$$[\boldsymbol{\Theta},\boldsymbol{\Omega}]\mathbf{h} \triangleq (\boldsymbol{\Theta}\boldsymbol{\Omega} - \boldsymbol{\Omega}\boldsymbol{\Theta})\mathbf{h} = (\boldsymbol{\vartheta}\times\boldsymbol{\omega})\times\mathbf{h}, \quad \text{for any } \mathbf{h}\in\mathbb{R}^3. \tag{3.15}$$

Therefore, formula (3.13) in terms of axial vectors becomes

$$(D\boldsymbol{\omega}\cdot\boldsymbol{\vartheta})\times\mathbf{h} = (\boldsymbol{\vartheta}' + \boldsymbol{\vartheta}\times\boldsymbol{\omega})\times\mathbf{h}, \quad \text{for any } \mathbf{h}\in\mathbb{R}^3 \tag{3.16}$$

The linearization of $\boldsymbol{K}$ now follows at once from $(3.9)_2$, (3.16) and the relation $\boldsymbol{K}_\varepsilon = \boldsymbol{\Lambda}_\varepsilon^T\boldsymbol{\omega}_\varepsilon$. The result is given by

$$(D\boldsymbol{K}\cdot\boldsymbol{\vartheta})\times\mathbf{h} = \left(\frac{d}{d\varepsilon}\Big|_{\varepsilon=0}\boldsymbol{K}_\varepsilon\right)\times\mathbf{h} = (\boldsymbol{\Lambda}^T\boldsymbol{\vartheta}')\times\mathbf{h}, \tag{3.17}$$

for any $\mathbf{h}\in\mathbb{R}^3$. The same result is obtained by expressing (3.14) in terms of axial vectors. Finally, the linearization of $\boldsymbol{\Gamma}$ may by obtained with the aid of the directional derivative formula; i.e.,

$$\begin{aligned} D\boldsymbol{\Gamma}\cdot\boldsymbol{\eta} \triangleq \frac{d}{d\varepsilon}\Big|_{\varepsilon=0}\boldsymbol{\Gamma}_\varepsilon &= \frac{d}{d\varepsilon}\Big|_{\varepsilon=0}(\boldsymbol{\Lambda}_\varepsilon\boldsymbol{\phi}_{0\varepsilon} - \mathbf{E}_3) \\ &= \boldsymbol{\Lambda}^T\left(\frac{d\boldsymbol{\eta}_0}{dS} - \boldsymbol{\vartheta}\times\frac{d\boldsymbol{\phi}_0}{dS}\right) \end{aligned} \tag{3.18}$$

Remark 3.2. Note that the *spatial* counterpart of the linearized *material* strain measures $D\boldsymbol{K}\cdot\boldsymbol{\vartheta}$ and $D\boldsymbol{\Gamma}\cdot\boldsymbol{\eta}$ is given by the expressions

$$\delta\boldsymbol{\omega}\cdot\boldsymbol{\vartheta} \triangleq \boldsymbol{\Lambda}D\boldsymbol{K}\cdot\boldsymbol{\vartheta}, \qquad \delta\boldsymbol{\gamma}\cdot\boldsymbol{\eta} \triangleq \boldsymbol{\Lambda}D\boldsymbol{\Gamma}\cdot\boldsymbol{\vartheta} \tag{3.19}$$

The complete analogy between (3.19) and (2.5) should be noted. ▪

For convenience, the linearization of the strain measures in the spatial and material descriptions is summarized in Box 3, where a superposed "prime" designates d/dS.

BOX 3. *Linearized strain measures* ($\eta \equiv (\eta_0, \vartheta) \in T_\phi C$)

spatial	material
$\delta\gamma \cdot \eta = \mathbf{u}' - \vartheta \times \mathbf{t}_3$	$D\Gamma \cdot \eta = \Lambda^T[\mathbf{u}' - \vartheta \times \phi'_0]$
$\delta\omega \cdot \vartheta = \vartheta'$	$DK \cdot \vartheta = \Lambda^T \vartheta'$

4. Weak form of balance equations. Tangent operator.

Consider again any arbitrary *admissible variation* $\eta(S) \equiv (\eta_0(S), \vartheta(S)) \in T_\phi C$. In what follows, attention is restricted to the static case. By multiplying the spatial local forms (2.6a,b) of the balance laws equations by $\eta(S)$ one obtains

$$G(\phi,\eta) \triangleq \int_{[0,L]} [(\frac{d\mathbf{n}}{dS} + \bar{\mathbf{n}}) \cdot \eta_0 + (\frac{d\mathbf{m}}{dS} + \frac{d\phi_0}{dS} \times \mathbf{n} + \bar{\mathbf{m}}) \cdot \vartheta] dS = 0 \qquad (4.1)$$

Since the variation $\eta(S) \in T_\phi C$ vanishes at the boundary, integration by parts of (4.1) leads to the so-called *spatial version of the weak form of momentum balance*, expressed as

$$G(\phi,\eta) = \int_{[0,L]} \{ \mathbf{n} \cdot [\frac{d\eta_0}{dS} - \vartheta \times \frac{d\phi_0}{dS}] + \mathbf{m} \cdot \frac{d\vartheta}{dS} \} dS - \int_{[0,L]} (\bar{\mathbf{n}} \cdot \eta_0 + \bar{\mathbf{m}} \cdot \vartheta) dS, \qquad (4.2)$$

for arbitrary $\eta \equiv (\eta_0, \vartheta) \in T_\phi C$. An entirely analogous procedure leads to the statement of the weak form of constitutive equations. However, henceforth we shall be mainly concerned with the development of a displacement type finite element formulation. Accordingly, we assume that constitutive equations (2.8) hold strongly, or point-wise.

To perform the linearization of the weak form of momentum balance, it is convenient to rephrase (4.2) in *material form*. By making use of relations (2.3) we obtain the following alternative (*material*) expression of (4.2)

$$G(\phi,\eta) = \int_{[0,L]} \left\{ \mathbf{N} \cdot \Lambda^T [\frac{d\eta_0}{dS} - \vartheta \times \frac{d\phi_0}{dS}] + \mathbf{M} \cdot \Lambda^T \frac{d\vartheta}{dS} \right\} dS - \int_{[0,L]} (\bar{\mathbf{n}} \cdot \eta_0 + \bar{\mathbf{m}} \cdot \vartheta) dS, \qquad (4.3)$$

for arbitrary $\eta \equiv (\eta_0, \vartheta) \in T_\phi C$.

4.1. Consistent Linearization. Tangent Operator.

A complete account of linearization procedures relevant to the problem at hand is given in Marsden & Hughes [1983, Chap. 4]. Here, we proceed in the context discussed in Section 3. Denote by $L[G(\hat{\phi},\eta)]$ the linear part of the functional $G(\phi,\eta)$ at the configuration $\phi = \hat{\phi}$; by definition we have

$$L[G(\hat{\phi},\eta)] = G(\hat{\phi},\eta) + DG(\hat{\phi},\eta) \cdot \Delta\phi \qquad (4.4a)$$

where, as in Section 3, the (Frechet) differential $DG(\hat{\phi},\eta)$ is obtained through the directional derivative formula

$$DG(\hat{\boldsymbol{\phi}},\boldsymbol{\eta})\cdot\Delta\boldsymbol{\phi} \;=\; \frac{d}{d\varepsilon}\bigg|_{\varepsilon=0} G(\hat{\boldsymbol{\phi}}+\varepsilon\Delta\boldsymbol{\phi},\,\boldsymbol{\eta}), \tag{4.4b}$$

and $\Delta\boldsymbol{\phi}\equiv(\mathbf{u}_0,\boldsymbol{\psi})\in T_{\boldsymbol{\phi}}C$ is an admissible variation. The physical interpretation of (4.4a) is standard. The term $G(\hat{\boldsymbol{\phi}},\boldsymbol{\eta})$ supplies the *unbalanced force* at the configuration $\hat{\boldsymbol{\phi}}\in C$ and the term $DG(\hat{\boldsymbol{\phi}},\boldsymbol{\eta})\cdot\Delta\boldsymbol{\phi}$, *linear* in $\Delta\boldsymbol{\phi}$, yields the so-called *tangent stiffness*. Of course, if $\hat{\boldsymbol{\phi}}\in C$ is an equilibrium configuration, we must have $G(\hat{\boldsymbol{\phi}},\boldsymbol{\eta}) = 0$ for any $\boldsymbol{\eta}\in T_{\boldsymbol{\phi}}C$.

The weak form (4.3) may be rephrased in a more compact form by introducing the following notation. Define *material* and *spatial* vectors of resultant stresses and stress couples, $\mathbf{R}$ and $\mathbf{r}$, by setting

$$\mathbf{R}=\begin{Bmatrix}\mathbf{N}\\ \mathbf{M}\end{Bmatrix},\quad \mathbf{r}=\begin{Bmatrix}\mathbf{n}\\ \mathbf{m}\end{Bmatrix}\equiv\Pi\mathbf{R},\quad \text{where}\quad \Pi\triangleq\begin{bmatrix}\Lambda & \mathbf{0}\\ \mathbf{0} & \Lambda\end{bmatrix} \tag{4.5}$$

In addition, introduce a matrix differential operator Ξ defined as

$$\Xi^T\triangleq\begin{bmatrix}\dfrac{d}{dS}\mathbf{1} & [\boldsymbol{\phi}'_0\times]\\ \mathbf{0} & \dfrac{d}{dS}\mathbf{1}\end{bmatrix} \tag{4.6a}$$

Here, $(\cdot)'$ denotes differentiation with respect to S, $\dfrac{d}{dS}\mathbf{1}$ is the block diagonal operator defined below, and $\mathbf{1} = Diag\,[1, 1, 1]$ is the indentity matrix. In addition, $[\boldsymbol{\phi}'_0\times]$ is the skew-symmetric matrix associated with the axial vector $\boldsymbol{\phi}'_0 = \boldsymbol{\phi}'_{0i}\,\mathbf{e}_i$; i.e.,

$$[\boldsymbol{\phi}'_0\times]\triangleq\begin{bmatrix}0 & -\boldsymbol{\phi}'_{03} & \boldsymbol{\phi}'_{02}\\ \boldsymbol{\phi}'_{03} & 0 & -\boldsymbol{\phi}'_{01}\\ -\boldsymbol{\phi}'_{02} & \boldsymbol{\phi}'_{01} & 0\end{bmatrix},\qquad \frac{d}{dS}\mathbf{1}\triangleq Diag\,[\frac{d}{dS},\frac{d}{dS},\frac{d}{dS}] \tag{4.6b}$$

With this notation at hand, equation (4.3) may then be recast as

$$G(\boldsymbol{\phi},\boldsymbol{\eta}) \;=\; \int_{[0,L]}[(\Xi^T\boldsymbol{\eta})\cdot(\Pi\mathbf{R}) \;-\; \boldsymbol{\eta}\cdot\bar{\mathbf{r}}]\,dS \tag{4.7}$$

where $\bar{\mathbf{r}}^T\triangleq\{\bar{\mathbf{n}},\,\bar{\mathbf{m}}\}^T$. To obtain the linear part (4.4) of (4.7) we need to obtain the expression for the linearized constitutive equations. First, note that with the aid of Ξ defined by (4.6a) the results in Box 2 may be expressed as

$$\begin{Bmatrix}D\boldsymbol{\Gamma}\cdot\mathbf{u}\\ D\boldsymbol{K}\cdot\boldsymbol{\vartheta}\end{Bmatrix} \;=\; \hat{\Pi}^T\,\hat{\Xi}^T\begin{Bmatrix}\mathbf{u}_0\\ \boldsymbol{\psi}\end{Bmatrix} \;\equiv\; \hat{\Pi}^T\,\hat{\Xi}^T\,\Delta\boldsymbol{\phi}, \tag{4.8}$$

Thus, on account of (2.9), the linearized internal force is given by

$$D\mathbf{R}\cdot\Delta\boldsymbol{\vartheta} \;=\; \hat{\mathbf{C}}\begin{Bmatrix}D\boldsymbol{\Gamma}\cdot\mathbf{u}\\ D\boldsymbol{K}\cdot\boldsymbol{\psi}\end{Bmatrix} \;=\; \hat{\mathbf{C}}\,\hat{\Pi}^T\,\hat{\Xi}^T\,\Delta\boldsymbol{\phi}, \tag{4.9}$$

where $\hat{\mathbf{C}}$ is the (material) tangent elasticity tensor given by (2.9). Note that $\hat{\Lambda}$, $\hat{\Pi}$, and $\hat{\Xi}$ represent the quantities Λ, Π, and Ξ evaluated at $\boldsymbol{\phi} = \hat{\boldsymbol{\phi}}$. Linearization of (4.7) leads to :

$$DG(\hat{\boldsymbol{\phi}},\boldsymbol{\eta})\cdot\Delta\boldsymbol{\phi} \;=\; D_1G(\hat{\boldsymbol{\phi}},\boldsymbol{\eta})\cdot\Delta\boldsymbol{\phi} + D_2G(\hat{\boldsymbol{\phi}},\boldsymbol{\eta})\cdot\Delta\boldsymbol{\phi} \tag{4.10}$$

The first term in (4.10) is due to linearization of the internal force $\mathbf{R}$, and corresponds to the *material* part of the tangent stiffness matrix. The second

term gives rise to the *geometric* part of the tangent stiffness matrix, and results from the linearization of the operator $[\tilde{\Xi}\,\Pi]$ defined in (4.6). For the first term in (4.10) we have

$$D_1G(\hat{\phi},\eta)\cdot\Delta\phi = \int_{[0,L]} (\hat{\Xi}^T\eta)\cdot(\hat{\mathbf{c}}\,\hat{\Xi}^T\Delta\phi)\,dS, \tag{4.11}$$

where $\hat{\mathbf{c}} \triangleq \hat{\Pi}\,\mathbf{C}\,\hat{\Pi}^T$ is the *spatial* form of the elasticity tensor. The second term in (4.10) may be expressed as

$$D_2G(\hat{\phi},\eta)\cdot\Delta\phi = \int_{[0,L]} (\Psi^T\eta)\cdot(\hat{\mathbf{B}}\,\Psi^T\Delta\phi)\,dS \tag{4.12}$$

where, Ψ is a matrix differential operator defined as follows

$$\Psi \triangleq \begin{bmatrix} \frac{d}{dS}1 & 0 & 0 \\ 0 & \frac{d}{dS}1 & 1 \end{bmatrix}, \tag{4.13}$$

and $\mathbf{B}$ is the so-called *geometric stiffness matrix* which for the problem at hand takes the form †

$$\mathbf{B} \triangleq \begin{bmatrix} \mathbf{0} & \mathbf{0} & [-\mathbf{n}\times] \\ \mathbf{0} & \mathbf{0} & [-\mathbf{m}\times] \\ [\mathbf{n}\times] & \mathbf{0} & [\mathbf{n}\otimes\phi'_0 - (\mathbf{n}\cdot\phi'_0)1] \end{bmatrix} \tag{4.14}$$

In (4.12), $\hat{\mathbf{B}}$ denotes the matrix $\mathbf{B}$ evaluated at $\phi=\hat{\phi}$. Recall that $[(\cdot)\times]$ denotes the *skew-symmetric* matrix whose axial vector is given by $(\cdot)$. Inspection of (4.14) reveals that the geometric stiffness $\mathbf{B}$ is generally non-symmetric. Hence, it appears that the *geometric tangent operator* given by (4.12) *is non-symmetric.* We show next that this is indeed the case *only if the configuration* $\hat{\phi}\in C$ *is not an equilibrium configuration.*

4.2. Symmetry of the tangent operator at equilibrium. Potential.

To examine the nature of the lack in symmetry of the tangent $DG(\hat{\phi},\eta)\cdot\Delta\phi$ we consider the skew-symmetric part given by

$$[DG(\hat{\phi},\eta)\cdot\Delta\phi]^A \triangleq D_2G(\hat{\phi},\eta)\cdot\Delta\phi - D_2G(\hat{\phi},\Delta\phi)\cdot\eta \equiv \int_{[0,L]} (\Psi^T\eta)\cdot(\hat{\mathbf{B}}^A\,\Psi^T\Delta\phi)\,dS \tag{4.15}$$

where $\hat{\mathbf{B}}^A \triangleq \tfrac{1}{2}(\hat{\mathbf{B}}-\hat{\mathbf{B}}^T)$. Since by construction $\eta\equiv(\eta_0,\vartheta)$ and $\Delta\phi\equiv(\mathbf{u}_0,\psi)$, expanding (4.15) we have

$$\begin{aligned}
[DG(\hat{\phi},\eta)\cdot\Delta\phi]^A &= \int_{[0,L]} \{\mathbf{m}\cdot[\vartheta\times\psi' - \psi\times\vartheta'] + \mathbf{n}\cdot[\psi\times(\vartheta\times\hat{\phi}'_0) - \vartheta\times(\psi\times\hat{\phi}'_0]\}\,dS \\
&= \int_{[0,L]} \{\mathbf{m}\cdot(\vartheta\times\psi)' + \mathbf{n}\cdot[(\psi\cdot\hat{\phi}'_0)\vartheta - (\vartheta\cdot\hat{\phi}'_0)\psi]\}\,dS \\
&= \int_{[0,L]} \{\mathbf{m}\cdot(\vartheta\times\psi)' - \mathbf{n}\cdot[(\vartheta\times\psi)\times\hat{\phi}'_0]\}\,dS
\end{aligned} \tag{4.16}$$

Integration by parts of (4.16) finally yields

$$\begin{aligned}
[DG(\hat{\phi},\eta)\cdot\Delta\phi]^A = &- \int_{[0,L]} [\mathbf{m}' + \hat{\phi}'_0\times\mathbf{n} + \bar{\mathbf{m}}]\cdot(\vartheta\times\psi)\,dS \\
&+ \int_{[0,L]} \bar{\mathbf{m}}\cdot(\vartheta\times\psi)\,dS + [\mathbf{m}\cdot(\vartheta\times\psi)]\Big|_{S\in\{0,L\}}
\end{aligned} \tag{4.17}$$

†Note that in component form $[\mathbf{n}\otimes\phi_0]_{ij} = n_i\,\phi_{0j}$.

It follows that for our choice of $T_\phi C$ given by (3.5) $\mathbf{m}\cdot(\vartheta\times\psi)\big|_{S\in\{0,L\}} = 0$. In addition, the first term in (4.17) is simply the weighted form of the the static version of the local balance of angular momentum equation (2.6b). Accordingly, this term vanishes at an equilibrium configuration. Thus, (4.17) vanishes identically provided that $\overline{\mathbf{m}} \equiv 0$ point-wise in $(0,L)\subset\mathbb{R}$ and the configuration is in equilibrium.

Remark 4.1. The condition of no distributed moment $\overline{\mathbf{m}} \equiv 0$, appears to be in agreement with the fact pointed out by Ziegler [1977] and elaborated upon by Argyris and co-workers [1978,1980,1982], that loading by "moments with fixed axes" is non-conservative. Note that although ψ and ϑ are admissible (infinitesimal) rotations, $\vartheta\times\psi$ is *not* an admissible infinitesimal rotation. Nevertheless, the *boundary* term $\mathbf{m}\cdot(\vartheta\times\psi)\big|_{S\in\{0,L\}} = 0$ in (4.17) *vanishes identically* for most boundary conditions of practical interest, such as simply supported, clamped, or free end. Other boundary conditions which result in cancellation of this boundary term are possible. However, this term does *not* vanish for the case of an *applied end moment with "fixed spatial axis,"* and thus this type of loading is non-conservative (see, e.g., Argyris and co-workers [1978]). The condition of conservative loading expressed by

$$\int_{[0,L]} \overline{\mathbf{m}}\cdot(\vartheta\times\psi)\,dS + [\mathbf{m}\cdot(\vartheta\times\psi)]\big|_{S\in\{0,L\}} = 0 \tag{4.18}$$

is analogous in structure to that arising in pressure dependent loading (Bufler [1984], Schweizerhof & Ramm [1984]). ▪

In view of expression (4.17) the following conclusion can be stated

(i) At an *equilibrium* configuration, the symmetry of the tangent stiffness depends solely upon external loading and boundary conditions; e.g., depends on whether the loading is conservative. The possible lack of symmetry at an equilibrium configuration is not related in any way to the presence of the classical rotation group SO(3) in the configuration space. The fact that a potential exists if (4.17) vanishes is the result of a well-known theorem due to Vainberg (see Marsden & Hughes [1983, Sec. 1.7] for a discussion in the general context of manifolds).

(ii) At a *non-equilibrated* configuration, the tangent operator is *non-symmetric* in general, even for conservative loading. The reason for this is again found in the fact that the configuration space C is a *manifold*. This conclusion is a particular instance of a general result in analysis in manifolds discussed below.

Remark 4.2. (*Potentials*) Assume in what follows that $\overline{\mathbf{m}} \equiv 0$ in $(0, L)$, and for simplicity let us consider the boundary condition in (3.5). Within the general context of the dynamic problem, the following functional $\Pi : C \to \mathbb{R}$ defined by

$$\Pi(\mathbf{w}, \phi) \triangleq T(\dot{\phi}_0, \mathbf{w}) + \int_{[0,L]} \Psi(\Gamma, K)\,dS - \int_{[0,L]} \overline{\mathbf{n}}\cdot\phi_0\,dS \tag{4.19a}$$

where

$$T(\dot{\phi}_0, \mathbf{w}) \triangleq \tfrac{1}{2}\int_{[0,L]} \rho A\,\|\dot{\phi}_0\|^2\,dS + \tfrac{1}{2}\int_{[0,L]} \rho\,(\mathbf{w}\cdot\mathbf{I}\mathbf{w})\,dS\,, \tag{4.19b}$$

furnishes the total energy (Hamiltonian) of the system. Here, $T(\dot{\phi}_0, \mathbf{w})$ is the kinetic energy of the rod, and $\psi(\Gamma, K)$ is a properly invariant (see, Antman [1972]) stored energy function, an example of which is given by

$$\psi(\Gamma, K) = \tfrac{1}{2}\begin{bmatrix}\Gamma^T & K^T\end{bmatrix} Diag\,[GA_1, GA_2, EA, EI_1, EI_2, GJ]\begin{Bmatrix}\Gamma\\ K\end{Bmatrix} \tag{4.20}$$

For the static case, the first variation of (4.19a) yields the weak form (4.3), and the second variation about a configuration $\hat{\boldsymbol{\phi}} \in C$ leads to the linearized weak form (4.10). The critical points of $\Pi(\boldsymbol{\phi})$ are the *equilibrium* configurations $\hat{\boldsymbol{\phi}}$.

A general result of analysis in manifolds states that the second variation of a map $\Pi: C \to \mathbb{R}$ is symmetric at the critical points of Π (Spivac [1982, pag.241]). Indeed, the Hessian of Π makes sense only at the critical points of Π (Abraham and Marsden [1978]). This general result is in agreement with conclusions (i) and (ii), in the sense that at an equilibrium configuration the tangent stiffness is symmetric. ▪

5. Finite Element Formulation.

In this section we consider the finite element formulation of the variational equations discussed in Section 4. Our treatment makes use of uniformly reduced integration on the pure displacement weak form, to avoid shear locking. For the linear problem the equivalence between uniformly reduced integrated forms and mixed methods is well known; (see, e.g. Stolarski et. al. [1984] where the equivalence with alternative approaches such as the "mode decomposition technique is also shown). For the finite deformation plane problem, the equivalence with mixed methods has been dealt with by Noor and coworkers [1981]. Notice that for the one dimensional problem no spurious zero energy modes appear as a result of reduced integration. This is in sharp contrast with the plate or shell problem (e.g., see Hughes & Tezduyar [1980], Criesfield [1984], Belytschko, Stolarsky & Carpenter [1984]). Details pertaining to the discretization and finite element arrays will be considered first. The update procedure which plays a crucial role in the formulation, is examined subsequently.

5.1. Discretization and F.E. arrays.

Consider a standard finite element discretization $[0,L] = \bigcup_{e=1}^{E} I_e^h$, where $I_e^h \subset [0,L]$ denotes a typical element with length $h > 0$, and E is the total number of elements. The space of admissible variations $T_{\boldsymbol{\phi}}C$ is approximated by a finite dimensional subspace $V^h \subset T_{\boldsymbol{\phi}}C$. As usual, the calculations are performed on an element basis. Accordingly, let $\Delta\boldsymbol{\phi}_e^h$ be the restriction to a a typical element I_e^h of the incremental displacement field-rotation field $\Delta\boldsymbol{\phi}^h \equiv (\mathbf{u}_0^h, \boldsymbol{\vartheta}^h) \in V^h$ superposed onto the configuration $\boldsymbol{\phi} \equiv (\boldsymbol{\phi}_0, \boldsymbol{\Lambda}) \in C$. The *incremental displacement-rotation* field $\Delta\boldsymbol{\phi}_e^h$ is then interpolated in terms of shape the functions according to

$$\mathbf{u}_{0e}^h(S) = \sum_{I=1}^{nel} N_I(S)\mathbf{u}_I^h; \quad \boldsymbol{\vartheta}_e^h(S) = \sum_{I=1}^{nel} N_I(S)\boldsymbol{\vartheta}_I^h \tag{5.1}$$

Here, *nel* represents the number of nodes of the beam element I_e^h, $N_I(S)$ the shape function associated with node I, and $\mathbf{u}_I^h$, $\boldsymbol{\vartheta}_I^h$ are the nodal incremental displacement and vorticity of element I_e^h at node I.

Computation of the out-of-balance force. The element contribution to the residual force vector is obtained from the discrete approximation to the weak form of momentum balance. Proceeding in a element fashion, by introducing (5.1) the discrete approximation to $G(\hat{\boldsymbol{\phi}}, \boldsymbol{\eta})$ may be written as

$$G^h(\hat{\boldsymbol{\phi}}, \boldsymbol{\eta}^h) = \sum_{e=1}^{E} G_e^h(\hat{\boldsymbol{\phi}}, \boldsymbol{\eta}^h) \tag{5.2a}$$

where

$$G_e^h(\hat{\boldsymbol{\phi}}, \boldsymbol{\eta}^h) = \boldsymbol{\eta}_e^h \cdot \mathbf{P}_e^h(\hat{\boldsymbol{\phi}}) \equiv \sum_{I=1}^{nel} \boldsymbol{\eta}_I^h \cdot \mathbf{P}_{eI}^h(\hat{\boldsymbol{\phi}}) \tag{5.2b}$$

Here, $\mathbf{P}_e^h(\hat{\boldsymbol{\phi}})$ denotes the unbalanced force vector in a typical element I_e^h, which is computed by evaluating the discrete approximations to Ξ, Π and $\mathbf{R}$ entering in expression (4.7). Let $\hat{\Xi}_I^h$ represent the *discrete* differential operators $\hat{\Xi}$ associated with node I. Substitution of (5.1) into (4.6a) yields

$$\hat{\Xi}_I^h = \begin{bmatrix} N_I'1 & \mathbf{0} \\ -N_I[\hat{\boldsymbol{\phi}}'_0\times] & N_I'1 \end{bmatrix} \tag{5.3}$$

In these expressions, N_I' denotes the derivative of $N_I(S)$ with respect to $S \in I_e^h$, $1 \equiv Diag[1\ 1\ 1]$ is the rank-3 unit matrix, and $[\hat{\boldsymbol{\phi}}'_0\times]$ is a skew-symmetric matrix whose axial vector is $\hat{\boldsymbol{\phi}}'_0$, as indicated in $(4.6b)_1$. Now assume that the *spatial* stress vector $\mathbf{r}_e^h = [\mathbf{n}_e^h \quad \mathbf{m}_e^h]$ is computed from the constitutive equations (2.7) in the manner described in Section 5.2 below, and let $\mathbf{P}_{eI}^h$ be the unbalanced nodal force in element I_e^h related to node I. We have the following expression

$$\mathbf{P}_{eI}^h(\hat{\boldsymbol{\phi}}) = \int_{I_e^h} \left[\hat{\Xi}_I \begin{Bmatrix} \mathbf{n}_e^h \\ \mathbf{m}_e^h \end{Bmatrix} - \begin{bmatrix} N_I 1 & \mathbf{0} \\ \mathbf{0} & N_I 1 \end{bmatrix} \begin{Bmatrix} \bar{\mathbf{n}} \\ \bar{\mathbf{m}} \end{Bmatrix} \right] dS \tag{5.4}$$

This completes the computation of the local residual vector.

Computation of the tangent stiffness matrix. We consider next the linearized weak form (4.10). The linear part of the weak form (5.5b) relative to element I_e^h at the configuration $\hat{\boldsymbol{\phi}}$ may be expressed as

$$L[G_e^h(\hat{\boldsymbol{\phi}}, \boldsymbol{\eta}^h)] \triangleq \boldsymbol{\eta}^h \cdot [\{\mathbf{S}_e^h(\hat{\boldsymbol{\phi}}) + \mathbf{T}_e^h(\hat{\boldsymbol{\phi}})\}\Delta\boldsymbol{\phi}_e^h + \mathbf{P}_e^h(\hat{\boldsymbol{\phi}})] \tag{5.5}$$

where $\mathbf{S}_e^h$ and $\mathbf{T}_e^h$ represent respectively the element stiffness matrix and element geometric stiffness matrix. Then $\{\mathbf{S}_e^h(\hat{\boldsymbol{\phi}}) + \mathbf{T}_e^h(\hat{\boldsymbol{\phi}})\}$ is the tangent stiffness matrix of the element I_e^h at the configuration $\hat{\boldsymbol{\phi}}$. Let $\mathbf{S}_{eIJ}^h$ and $\mathbf{T}_{eIJ}^h$ denote the submatrices coupling node I and J in $\mathbf{S}_e^h$ and $\mathbf{T}_e^h$, respectively. From (4.11) we have the expression

$$\mathbf{S}_{eIJ}^h = \int_{I_e^h} \hat{\Xi}_I^h \, \mathbf{c}_e^h \, \hat{\Xi}_J^{hT} \, dS \tag{5.6}$$

where $\hat{\Xi}_I^h$ is given by (5.3), and $\mathbf{c}_e$ are the *spatial* tangent elastic moduli. For the particular model (2.10), for instance, we have $\mathbf{c}_e^h = \Pi^h \mathbf{C} \Pi^{hT}$.

The geometric tangent stiffness is obtained by evaluating the geometric contribution to the tangent stiffness given by (4.12). For this purpose, first note that from (5.1) and (4.13) the discrete approximation to the operator Ψ in (4.12) is given by

$$\Psi_I^h = \begin{bmatrix} N_I'1 & \mathbf{0} & \mathbf{0} \\ \mathbf{0} & N_I'1 & N_I 1 \end{bmatrix} \tag{5.7}$$

Making use of expression (4.14) for the matrix $\mathbf{B}$, the geometric stiffness matrix takes the form

$$\mathbf{T}_{eIJ}^h = \int_{I_e^h} \Psi_I^h \mathbf{B}_e^h \Psi_J^h \, dS$$

$$= \int_{I_e^h} \begin{bmatrix} \mathbf{0} & -[\hat{\mathbf{n}}^h\times]N_I'N_J \\ [\hat{\mathbf{n}}^h\times]N_IN_J' & \{-[\hat{\mathbf{m}}^h\times]N_I'N_J + [\hat{\mathbf{n}}^h \otimes \hat{\boldsymbol{\phi}}'_0 - (\hat{\mathbf{n}}^h\cdot\hat{\boldsymbol{\phi}}'_0)1]N_IN_J\} \end{bmatrix} dS \tag{5.8}$$

We recall again that in this expression $[(\cdot)\times]$ is a rank-3 skew-symmetric matrix whose axial vector is $(\cdot)$. It should be noted that the submatrix "[2,2]" of $\mathbf{T}_e^h$ leads to an *unsymmetric* geometric stiffness matrix if the configuration $\hat{\phi}$ *is not in equilibrium.* At an equilibrium configuration the geometric stiffness becomes symmetric, in agreement with our discussion of Section 4.† Next, we proceed to discuss the update procedure and the solution scheme for the equilibrium configuration based on a Newton-Raphson strategy.

5.2. Configuration and stress update algorithm.

Assume the configuration $\boldsymbol{\phi}_n \equiv (\boldsymbol{\phi}_{0n}, \boldsymbol{\Lambda}_n) \in C$ is known. In a typical iterative solution procedure, one linearizes the weak form (4.7) about $\boldsymbol{\phi}_n \in C$ and solves the linearized weak form (4.4a) for an incremental deformation $\Delta\boldsymbol{\phi} \equiv (\mathbf{u}_0, \boldsymbol{\vartheta}) \in T_{\boldsymbol{\phi}} C$, where $\boldsymbol{\vartheta}$ is the axial vector (incremental rotation) of the skew-symmetric tensor $\boldsymbol{\Theta}$. An update procedure which is consistent with the geometric structure of the problem (embedded in the definition of the configuration space C) is given by the formulae

$$\boldsymbol{\phi}_{0n+1}(S) = \boldsymbol{\phi}_{0n}(S) + \mathbf{u}_0(S), \qquad \boldsymbol{\Lambda}_{n+1}(S) = \exp[\boldsymbol{\Theta}(S)]\boldsymbol{\Lambda}_n(S) \tag{5.9}$$

Note that this update is in fact the only possible one that furnishes an updated configuration $\boldsymbol{\phi}_{n+1} \equiv (\boldsymbol{\phi}_{0n+1}, \boldsymbol{\Lambda}_{n+1})$ which belongs to the configuration space C. Note also that the exponential of the (skew-symmetric) incremental rotation, $\exp[\boldsymbol{\Theta}]$, is given in *closed form* by formula (*) in Box 4.

Remark 5.1. The geometric interpretation of the update formula (5.9) is illustrated in Fig. 3.1. The admissible configurations are symbolically represented by points in the surface C. $\boldsymbol{\Theta}$ defines an incremental rotation; i.e., an element in the tangent plane at $\boldsymbol{\Lambda}_n$. The updated configuration $\boldsymbol{\Lambda}_{n+1}$ is obtained by projecting $\boldsymbol{\Lambda}$ onto C by means of the exponential map. A dual construction can be performed in the reference configuration in terms of $\boldsymbol{\Theta}^M = \boldsymbol{\Lambda}^T \boldsymbol{\Theta} \boldsymbol{\Lambda}$, as explained in remark 3.1. ▪

It remains to compute the updated *spatial* and *material* curvatures $\boldsymbol{\Omega}_{n+1}$ and $\mathbf{K}_{n+1}$; or, equivalently, its axial vectors $\boldsymbol{\omega}_{n+1}$ and $\boldsymbol{K}_{n+1}$. This calculation involves the derivative of the exponential of a skew-symmetric matrix. The result, quoted in Box 4, takes a remarkably simple form and is justified in Appendix I.

Remark 5.2. It is noted that $(d\boldsymbol{\Theta}(S)/dS)\exp[\boldsymbol{\Theta}(S)]$, furnishes only a *first order approximation* to $\{d\exp[\boldsymbol{\Theta}(S)]/dS\}$. Expression (3.12) is in agreement with this fact. However, as indicated in Box 4, the *exact* expression involves the commutator of $\boldsymbol{\Theta}$ and $\boldsymbol{\Theta}'$ (see also Appendix I). In order to preserve the overall accuracy of the process it is essential to employ the exact expression. Its *conceptual* simplicity resulting from the formula (*) for the exponential is noted.

Remark 5.3. It should be noted that $\bar{\boldsymbol{\vartheta}}$ defined as

$$\mathbf{e} = \frac{\boldsymbol{\vartheta}}{\|\boldsymbol{\vartheta}\|}, \qquad \bar{\boldsymbol{\vartheta}} = \tan(\|\boldsymbol{\vartheta}\|/2)\,\mathbf{e} \tag{5.10}$$

blows up when $\|\boldsymbol{\vartheta}\|$ is in the vicinity of $(2n+1)\pi$ $(n = 0,1,2,\ldots)$, and the formula (*) for the exponential in Box 4 becomes singular as $\|\boldsymbol{\vartheta}\| \to (2n+1)\pi$. Thus, in practical implementations the optimal parametrization of the section rotation is

† In the case where structural displacements stay in a plane, we have a symmetric geometric stiffness matrix even if the configuration is not in equilibrium. The reason for this is that the configuration space becomes a linear space (recall that $SO(2)$ is isomorphic to R). A physical motivation is found in the fact that finite rotations commute when the axis of rotation remains fixed (normal to the plane of the structure).

BOX 4. *Configuration and stress update: Conceptual algorithm*

- Compute *axial vectors*

$$\mathbf{e} = \frac{\boldsymbol{\vartheta}}{\|\boldsymbol{\vartheta}\|} \qquad \bar{\boldsymbol{\vartheta}} = \tan(\|\boldsymbol{\vartheta}\|/2)\,\mathbf{e}$$

$$\bar{\boldsymbol{\vartheta}}' = \tfrac{1}{2}\frac{\tan(\|\boldsymbol{\vartheta}\|/2)}{\|\boldsymbol{\vartheta}\|/2}[\boldsymbol{\vartheta}' - (1 - \frac{\|\boldsymbol{\vartheta}\|}{\sin\|\boldsymbol{\vartheta}\|})(\mathbf{e}\cdot\boldsymbol{\vartheta}')\,\mathbf{e}]$$

- Compute exponential and derivative

$$\exp[\boldsymbol{\Theta}(S)] = \mathbf{I} + \frac{2}{1+\|\bar{\boldsymbol{\vartheta}}\|^2}(\bar{\boldsymbol{\Theta}} + \bar{\boldsymbol{\Theta}}^2) \quad (*)$$

$$(\frac{d\exp[\boldsymbol{\Theta}]}{dS})\exp[-\boldsymbol{\Theta}] = \frac{2}{1+\|\bar{\boldsymbol{\vartheta}}\|^2}(\bar{\boldsymbol{\Theta}}' + \bar{\boldsymbol{\Theta}}'\,\bar{\boldsymbol{\Theta}} - \bar{\boldsymbol{\Theta}}\,\bar{\boldsymbol{\Theta}}')$$

- Update the configuration

$$\boldsymbol{\phi}_{0n+1} = \boldsymbol{\phi}_{0n} + \mathbf{u}_0$$

$$\boldsymbol{\Lambda}_{n+1} = \exp[\boldsymbol{\Theta}]\,\boldsymbol{\Lambda}_n$$

- Compute curvature and strains

$$\boldsymbol{\Omega}_{n+1} = \frac{d\exp[\boldsymbol{\Theta}]}{dS}\exp[-\boldsymbol{\Theta}] + \exp[\boldsymbol{\Theta}]\,\boldsymbol{\Omega}_n\exp[-\boldsymbol{\Theta}]$$

$$\boldsymbol{K}_{n+1} = \boldsymbol{\Lambda}_{n+1}^T\,\boldsymbol{\Omega}_{n+1}$$

$$\boldsymbol{\Gamma}_{n+1} = \boldsymbol{\Lambda}_{n+1}\,\boldsymbol{\phi}'_{0n+1} - \mathbf{E}_3$$

- Calculate stress resultants and stress couples

$$\mathbf{N}_{n+1} = \frac{\partial\Psi(\boldsymbol{\Gamma}_{n+1}, \boldsymbol{K}_{n+1})}{\partial\boldsymbol{\Gamma}} \qquad \mathbf{M}_{n+1} = \frac{\partial\Psi(\boldsymbol{\Gamma}_{n+1}, \boldsymbol{K}_{n+1})}{\partial\boldsymbol{K}}$$

furnished by the *four quaternion parameters*. In this connection, see the discussion of Kane et. al. [1983]. The details concerning the practical implementation of the update procedure based on the use of quaternions is discussed in Appendix II. We note that this implementation relies crucially on a singularity-free procedure for quaternion extraction as proposed by Spurrier [1978]. ▪

Remark 5.4. The rotation formula proposed by Hughes & Winget [1980], and further elaborated upon by Hughes [1984], furnishes only a *second order* approximation to the exact formula (*) in Box 4 obtained by setting

$$\frac{\tan(\|\boldsymbol{\vartheta}\|/2)}{\|\boldsymbol{\vartheta}\|/2} \approx 1 \quad \Rightarrow \quad \bar{\boldsymbol{\vartheta}} \approx \tfrac{1}{2}\boldsymbol{\vartheta} \tag{5.11}$$

The derivation of Hughes & Winget, however, is based on a direct approximation to the rate equation in Box 1 employing the mid-point rule. ▪

6. Extension to Non-conservative Problems.

Non-conservative loading can be accommodated easily within the present formulation. As an example, consider the case of a *follower* distributed load, denoted by $\mathbf{n}^{nc}$. Since this type of loading must follow the deformation of the

rod, $\mathbf{n}^{nc}$ is characterized by components relative to the moving frame $\{\mathbf{t}_I\}$ of the form

$$\mathbf{n}^{nc} \equiv N_I^{nc}\,\mathbf{t}_I, \qquad \text{where} \qquad N_I^{nc} \equiv CONST. \tag{6.1}$$

The contribution of $\mathbf{n}^{nc}$ to the weak form of momentum balance is then given in the standard manner as

$$G_{ext}^{nc} \equiv -\int_{[0,L]} \boldsymbol{\eta}_0 \cdot \mathbf{n}^{nc}\, dS \tag{6.2}$$

The contribution to the tangent stiffness operator can be easily computed by noting that, for any variation $\mathbf{u} \equiv (\mathbf{u}_0, \boldsymbol{\psi}) \in T_\phi C$ the moving frame $\{\mathbf{t}_I\}_{I=1,2,3}$ is "perturbed" according to

$$D\mathbf{t}_I \cdot \mathbf{u} \equiv \boldsymbol{\psi} \times \mathbf{t}_I, \qquad (I = 1,2,3) \tag{6.3}$$

Consequently, since $N_I^{nc} = CONST.$, it follows that $D\mathbf{n}^{nc} \cdot \mathbf{u} = \boldsymbol{\psi} \times \mathbf{n}^{nc}$, so that the contribution to the tangent stiffness becomes

$$DG_{ext}^{nc} = -\int_{[0,L]} \boldsymbol{\eta}_0 \cdot (\boldsymbol{\psi} \times \mathbf{n}^{nc})\, dS \equiv \int_{[0,L]} [\boldsymbol{\eta} \quad \boldsymbol{\vartheta}] \cdot \begin{bmatrix} \mathbf{0} & [\mathbf{n}^{nc} \times] \\ \mathbf{0} & \mathbf{0} \end{bmatrix} \begin{Bmatrix} \mathbf{u}_0 \\ \boldsymbol{\psi} \end{Bmatrix} dS \tag{6.4}$$

where, as in Section 4.1, $[(\cdot) \times]$ denotes the skew-symmetric matrix whose axial vector is $(\cdot)$. By introducing the finite element discretization $V^h \subset T_\phi C$ we have, for each element I_e^h

$$G_{ext}^{nc}\Big|_{I_e^h} = \sum_{I=1}^{nsl} \sum_{J=1}^{nsl} \boldsymbol{\eta}_I^h \cdot \mathbf{S}_{eIJ}^{nc}\, \mathbf{u}_J^h \tag{6.5}$$

where $\mathbf{S}_{eIJ}^{nc}$ is the so-called "load stiffness"" coupling nodes I and J and given by

$$\mathbf{S}_{eIJ}^{nc} = \int_{[0,L]} \begin{bmatrix} \mathbf{0} & -N_I N_J [\mathbf{n}^{nc} \times] \\ \mathbf{0} & \mathbf{0} \end{bmatrix} dS \tag{6.6}$$

Remark 6.1. The case of pressure loading, characterized by the condition that an applied distributed load remains *normal to the line of centroids* in all configurations, often arises in applications. This type of loading condition may be easily characterized by introducing a second moving frame $\{\mathbf{a}_1, \mathbf{a}_2, \mathbf{a}_3\}$ such that $\mathbf{a}_3$ is tangent to the deformed line of centroids. Accordingly, we may set

$$\mathbf{a}_3 \triangleq \frac{\boldsymbol{\phi}'_0}{\|\boldsymbol{\phi}'_0\|}, \quad \mathbf{a}_2 \triangleq \frac{[\mathbf{I} - \mathbf{a}_3 \otimes \mathbf{a}_3] : \mathbf{t}_2}{\|[\mathbf{I} - \mathbf{a}_3 \otimes \mathbf{a}_3] : \mathbf{t}_2\|}, \quad \mathbf{a}_1 \triangleq \mathbf{a}_2 \times \mathbf{a}_3 \tag{6.7}$$

The pressure loading may then be expressed as $\bar{\mathbf{n}} \equiv p\,\mathbf{a}_1 + q\,\mathbf{a}_2$. The contribution to the tangent stiffness may be computed with the aid of the directional derivative. ▪

7. Numerical Simulations

In this section, we consider a series of numerical simulations that illustrate the performance of the formulation described above. These applications show the quadratic rate of convergence obtained, even for very large load steps, in well documented examples. In the first four examples, attention is focused on the plane problem where the rotation field is easily described by means of a single rotation angle (Reissner [1972,1982], Simo et. al. [1984]). A basic objective then is to show that the proposed three dimensional parametrization of the rotation field exactly replicates the plane rotation. The last three examples, on the

other hand, are concerned with fully three-dimensional deformation, and have been considered in previous work (Bathe [1979], Argyris and co-workers [1979, 1981]). These examples demonstrate that symmetry of the tangent stiffness does *not* hold in the iteration process but is attained at the converged solution. Throughout all the examples discussed below, the constitutive model defined by (2.10) is considered.

Convergence of the finite element solution is established on the basis of the Euclidean norm of the out-of-balance force. A full Newton-Raphson iterative solution procedure is employed in all the calculations reported herein. Tracing of post-buckling diagrams throughout the simulations is accomplished by a generalized form of the classical arc-length method, (Riks [1972], Wempner [1971]) to include an arbitrary linear combination of degrees of freedom as constraint condition. The basic implementation of this procedure proceeds in two steps and is due to Schweizerhof, see Simo, Wriggers, Schweizerhof and Taylor [1984]. The first step involves the solution of the linearized problem under unit load. For the case of follower load, this unit load must be properly updated. It is emphasized that no special effort is made to optimize the total number of loading steps for a given calculation.

Example 7.1. *Pure bending of a cantilever beam.* A straight rod of unit length and bending stiffness $EI = 2.$ is subject to a concentrated end moment M. The finite element mesh consists of five elements with linear interpolation shape functions N_I. A one-point (uniformly reduced) quadrature is employed to compute all the arrays. The exact solution to this problem is a circular curve with radius $\rho = EI/M$. An applied end moment, $M = 4\pi$, will force the rod to deform into a full closed circle. In this example a moment *twice* this magnitude, i.e., $M = 8\pi$, is applied in *one load step*, making the rod wind around itself twice. Convergence to the exact solution is attained in *two iterations*. The final shape of the rod is depicted in Fig. 7.1. It is noted that the same performance, i.e., exact result in two iterations, is obtained for *any* magnitude of the applied end moment. The values of the residual norm throughout the iteration process are summarized below.

Iteration Number	*Euclidean Norm of Residual*
0	$0.251 \times 10^{+02}$ (8π)
1	$0.425 \times 10^{+02}$
2	0.441×10^{-13}

Example 7.2. *Cantilever beam subject to follower end load.* The material properties for this example, considered by Argyris & Symeonidis [1981], are $EI = 3.5 \times 10^7$ and $GA = 1.61538 \times 10^8$, and the total length is $L = 100$. The finite element mesh consists of *five* elements with quadratic shape functions. Two-point (uniformly reduced) Gauss intergration is used to compute all the arrays. For the purpose of tracing the load-deflection curve reported by Argyris & Symeonidis, a loading increment of 1000 was selected. The agreement found with these results is complete (see Figs. 7.2.*a* and 7.2.*b*). The characteristic quadratic convergence rate observed in a typical iteration of a load step is illustrated in the table below for the first loading step. Identical convergence rate was observed in subsequent load steps.

Iteration Number	*Euclidean Norm of Residual*
0	$0.100 \times 10^{+04}$
1	$0.542 \times 10^{+07}$
2	$0.270 \times 10^{+05}$
3	$0.583 \times 10^{+02}$
4	0.159×10^{-02}
5	0.197×10^{-06}

Example 7.3. *Clamped-hinged deep circular arch subject to point load.* This example has been considered by a number of authors (Noor & Peters [1981], Simo et. al. [1984]), and the exact solution based on the Kirchhoff-Love theory is given by DaDeppo and Schmidt [1975]. The solution shown in Fig. 7.3.*a* for various stages of deformation is obtained with 40 *linear isoparametric* elements. The plot of the vertical and horizontal displacements under the applied concentrated load is shown in Fig. 7.3.*b*. Load control is employed in the first eight load steps, each of them of magnitude 100. Subsequently, a combined displacement control/arch length control is employed. The calculation was completed in total number of 155 load steps. The analysis yields a value for the buckling load of 905.28. The exact value reported by DaDeppo and Schmidt [1975] is 897. A second limit point is found for a *negative value* of the applied load of −77.07. The global computed solution is in complete agreement with the solution first obtained for the entire post-buckling range in Simo et. al. [1984]. The convergence rate observed during a typical load step is shown below for the first load increment.

Iteration Number	*Euclidean Norm of Residual*
0	$0.100 \times 10^{+03}$
1	$0.553 \times 10^{+05}$
2	$0.325 \times 10^{+03}$
3	$0.309 \times 10^{+03}$
4	$0.990 \times 10^{+00}$
5	0.125×10^{-01}
6	0.920×10^{-08}

Example 7.4. *Buckling of a hinged right-angle frame under both fixed and follower point load.* This example, also considered by Argyris and Symeonidis [1981], is concerned with the loss of stability by divergence (as opposed to flutter) of the right angle frame shown in Fig. 7.4.*a*. The length of each leg is 120. The inertia and area of the cross section are respectively 2 and 6. The value of Young's modulus is 7.2×10^6; the value of Poisson's ratio is 0.3. The vertical point load is applied on the horizontal member at 24 units from its left end. Ten quadratic elements, 5 on each leg, are employed in the calculation. The deformed shapes are shown in Figs. 7.4.*a* and 7.4.*b*. The load-deflection curves are shown in Figs. 7.4.*c* and 7.4.*d*. Note that the entire post-buckling range is depicted in these figures, in contrast with the results reported Argyris & Symeonidis which are limited to the pre-buckling case. It is interesting to observe that the load-deflection curves for both conservative and non-conservative loading cross the zero-load axis at exactly the same values, as shown in Figs. 7.4.*c* and 7.4.*d*. These curves were traced after 43 load

increments for the fixed load case, and 99 load increments for the follower load case. As noted by Argyris & Symeonidis, the follower loading (non-conservative) has a positive effect of stabilizing the system and leads to a value of the buckling load of 35447 in contrast with the value of 18532 obtained for fixed loading (conservative).

Example 7.5. *Cantilever 45-degree bend subject to fixed and follower end load.* This example has been considered by Bathe and Bolourchi [1979] under fixed end load. The bend has a radius of 100 with a unit square cross section. The material properties are $E = 10^7$ and $G = 0.5\times10^7$. These authors performed the analysis for conservative loading only using 8 three-dimensional degenerated beam elements. In the present calculation 8 linear elements are used. For comparison purposes with the results reported in Bathe & Bolourchi the bend is subject to a sequence of *three* load increments of magnitude 300, 150 and 150. The results are summarized in the table below.

Load level	Number of Iterations	Tip displacement					
		Present			Bathe & Bolourchi [1979]		
		u	v	w	u	v	w
300	13	22.33	58.84	40.08	22.5	59.2	39.5
450	8	18.62	52.32	48.39	—	—	—
600	6	15.79	47.23	53.37	15.9	47.2	53.4

It should be noted that the final load of 600 was achieved in the present simulation in *three* load increments. This accounts for the large number of iterations (13) required to attain convergence. By contrast, the results reported in Bathe & Bolourchi were obtained after *sixty* equal load increments. A perspective view and a projection view of the deformed bend at various load levels are shown in Fig. 7.5.*a* and Fig. 7.5.*b*. The tip displacement versus applied load curve, shown in Fig. 7.5.*c*, is given up to a load level of 3000.

In addition to the loading discussed above, the bend also is analyzed for a *follower load.* The deformed configurations of the bend at various follower load levels are shown in Figs. 7.5.*d* and 7.5.*e* — compare these with Figs. 7.5.*a* and 7.5.*b*. The tip displacement versus applied load curve obtained for this non-conservative loading is shown in Fig. 7.5.*f*. It should be noted from Figs. 7.5.*c* and 7.5.*f* that the tip displacement increases monotonically with the load for fixed loading, whereas in the case of follower load the tip displacement reaches a maximum and then decreases. This effect is a consequence of the twist experienced by the bend as a result of the follower load.

Finally, a similar simulation is performed with both the consistent (non-symmetric) and the *symmetrized* element tangent stiffness matrices. The total load of 600 is applied in 8 equal load increments of magnitude 75. The purpose of the calculation is to show that *no significant loss* of asymptotic convergence rate results from using the symmetrized tangent matrix. This follows from our discussion in Section 4. The residual and energy norms shown below correspond to the fifth load increment.

Iteration	Non-symmetric	Symmetric	
number	*Residual norm*	*Residual Norm*	*Energy Norm*
0	$0.750 \times 10^{+02}$	$0.750 \times 10^{+02}$	$0.410 \times 10^{+03}$
1	$0.147 \times 10^{+06}$	$0.147 \times 10^{+06}$	$0.228 \times 10^{+05}$
2	$0.426 \times 10^{+03}$	$0.423 \times 10^{+03}$	$0.453 \times 10^{+01}$
3	$0.173 \times 10^{+04}$	$0.140 \times 10^{+04}$	$0.258 \times 10^{+01}$
4	$0.299 \times 10^{+01}$	$0.844 \times 10^{+00}$	0.950×10^{-04}
5	$0.177 \times 10^{+00}$	0.661×10^{-01}	0.269×10^{-08}
6	0.230×10^{-07}	0.190×10^{-04}	0.275×10^{-13}

Example 7.6. *Lateral buckling of a cantilever right-angle frame under end load.* This problem also has been analyzed by Argyris et. al. [1979]. The geometric characteristics of the frame are shown in Fig. 7.6.*a*. The value of Young's modulus is 71240; and the value of Poisson's ratio is 0.31. The extreme slenderness of the cross section, $\frac{thickness}{heigth} = \frac{1}{50}$, should be noted. The frame is subject to an in-plane fixed end load as shown in Fig. 7.6.*a*. Further, the frame is driven to the buckling mode by a perturbation load initially applied at the free end normal the plane of the frame. This perturbation is removed in a neighborhood of the buckling load, as shown in Fig. 7.6.*c*. A value of ≈ 1.09 is found for the critical load. The plot of end load versus lateral tip displacement of the frame shown in Fig. 7.6.*c*. is in agreement with the result reported by Argyris et. al. [1979]. The calculation is completed after a total number of 25 loading steps employing displacement control. Perspective and projection views of deformed centroidal line corresponding to the final value of the applied end load are shown in Figs. 7.6.*a* and 7.6.*b*.

Example 7.7. *Lateral buckling behavior of a hinged right-angle frame: Complete post-buckling diagram.* Our final example is concerned with the tracing of the complete post-buckling range of a hinged right-angle frame acted upon by in-plane end moments, as shown in Fig. 7.7.*a*. The degrees of freedom at the hinged ends are translation along the x direction and rotation about the z direction. The apex of the frame is constrained to lie in the y-z plane. Due to the symmetry of the problem, only half of the frame need be modeled. The problem at hand involves truly large three dimensional rotations and poses a severe test on the performance of the three dimensional rod model. As the rotation of the hinged end varies from 0° to 360°, the frame rotates out-of-plane about the axis connecting its supports and returns to its initial configuration. During the deformation process the legs of the frame experience significant amount of twist. This example was first proposed and analyzed by Argyris et. al. [1979] within the framework of a natural formulation based on the notion of *semi-tangential rotation*. Their analysis made use of 10 finite elements with *cubic* interpolation for the displacement field.

The present analysis based on the formulation described above, employs 10 finite elements with *quadratic* isoparametric interpolation for both displacement and rotation fields. Perspective and projection views of deformed configurations of the frame corresponding to various load levels are shown in Figs. 7.7.*b* and 7.7.*c*. Figure 7.7.*d* shows the plot of the abscissa of the left hinged end versus the load levels. The results of this analysis differ from those reported by Argyris and co-workers in the following. Upon returning to the

initial configuration, the applied end moment must be *identical in magnitude*, but with *reverse sign*, to the critical moment. Hence, the plot of the applied end moment versus lateral displacement of the apex must intersect symmetrically the moment axis. This is clearly the case for the curve shown in Fig. 7.7.*e*. The analogous curve reported in by Argyris et. al. [1979] violates this condition. The analysis is further pursued past this (negative) critical point and terminated upon completion of a second revolution of the frame about the line connecting its hinged ends. This results in the post-buckling diagram, completely *symmetric* relative to the moment axis, as depicted in Fig. 7.7.*e*. It is emphasized that at the end of the second revolution, the exact *positive critical value* of the applied end moment is recovered. Thus there no difficulty in subjecting the frame to any number of revolutions about the line connecting its supports. This would lead to the repeated tracing of the bifurcation diagram shown in Fig. 7.7.*e*..

Indeed after completion of the first revolution, the moment vs. lateral apex displacement plot intersects the moment axis at ≈ -626. A value of $\approx +626$ for this intersection point is found after completing the second revolution. Initially, a value of only 615.5 is obtained for the maximum moment due to the perturbation load. We recall that this perturbation load is removed subsequently.

The computational effort involved in the calculation for one revolution amounts to 160 loading steps, performed with a combined arc-length and displacement control algorithm. It is noted that the number of loading steps was not optimized.

The basic observation made in Section 4. concerning the *lack of symmetry* away from equilibrium, and *recovery of symmetry* at an equilibrium configuration, is numerically illustrated next. The table below shows the row norms of the skew-symmetric part of the global tangent stiffness at an arbitrarily selected load level. These results demonstrate lack of symmetry during the equilibrium iteration process, and confirm symmetry at the equilibrium configuration.

Iteration number	*Skew-symmetric part:* Row-Norm	*Out-of-Balance* Norm
0	1.7×10^{-08}	$0.100 \times 10^{+01}$
1	$1.1 \times 10^{+04}$	$0.784 \times 10^{+04}$
2	$6.9 \times 10^{+02}$	$0.354 \times 10^{+03}$
3	$6.2 \times 10^{+02}$	$0.347 \times 10^{+03}$
4	$1.9 \times 10^{+01}$	$0.108 \times 10^{+02}$
5	$1.6 \times 10^{+00}$	$0.807 \times 10^{+00}$
6	2.5×10^{-03}	0.141×10^{-02}
7	4.6×10^{-08}	0.322×10^{-07}

8. Closure.

The formulation developed in this paper is based on a fully nonlinear rod theory that allows for three dimensional finite rotation, and accounts for finite extension and shearing of the rod. The rotation and moment fields possess the usual physical meaning assigned in classical rod theories, such as the Kirchhoff-Love model; i.e., generally *non-commutative* orthogonal transformations. As a result, it has been shown that the consistent geometric tangent stiffness is *non-symmetric* for any configuration away from equilibrium. This lack of symmetry

concerns solely the rotational degrees of freedom, and is absent in the plane problem. It has also been proved that *full symmetry* always holds at equilibrium for conservative loading.

The practical implications of the lack of symmetry have been explored in numerical simulations employing Newton type of iterative solution schemes. Due to the localized character of this non-symmetry, and the full symmetry at equilibrium, it has been demonstrated that use of the symmetrized element tangent stiffness results in *no loss* of asymptotic rate of quadratic convergence.

Based on geometric considerations, an *exact* configuration update procedure has been developed. To avoid the singularity typically associated with parametrizations employing Euler angles or pseudo-vector of rotation, use has been made of *quaternion* parameters. This choice is optimal in the sense that singularity is avoided and storage requirements are minimized. Particular attention is given to the practical aspects involved in the implementation of the update procedure, such as the quaternion extraction from the orthogonal transformation matrix.

Follower loading is conveniently accounted for in the present formulation as a consequence of the representation of the section rotation by means of a moving orthogonal frame.

A number of numerical simulations have been documented to demonstrate the robustness of the proposed formulation. In particular, the performance of the symmetrized stiffness, the effectiveness of the update procedure, and the excellent rate of convergence have been illustrated throughout these simulations.

Acknowledgements

We thank Prof. Tudor Ratiu for his helpful discussions. This work was sponsored by the Air Force Office of Scientific Research under Grant No. AFOSR-83-0361. This support is gratefully acknowledged. Encouragement provided by Profs. K.S. Pister, E. Polak, and R.L. Taylor is also acknowledged.

References

Abraham, R. and J. E. Marsden, [1978], *Foundations of Mechanics*, 2nd. Ed., Addison-Wesley, Reading, Mass.

Antman, S.S., [1974], "Kirchhoff problem for nonlinearly elastic rods," *Quat. J. Appl. Math.* Vol XXXII, No.3, 221-240.

Antman, S.S., and K. B. Jordan [1975], "Qualitative aspects of the spatial deformation of non-linearly elastic rods," *Proc. Royal Society of Edinburg*, 73A, 5, 85-105

Antman, S.S., [1972], "The theory of rods," *Handbuch der Physik*, Vol. VIa/2, Springer-Verlag, Berlin.

Argyris J.H., H. Balmer, J. St. Doltsinis, P.C. Dunne, M. Haase, M. Kleiber, G.A. Malejannakis, J.P. Mlejenek, M. Muller and D.W. Scharpf [1979], "Finite Element Method -The natural approach," *Comp. Meth. Appl. Mech. Engrg.*, 17/18, 1-106.

Argyris. J.H. and Sp. Symeonides, [1981], "Nonlinear finite element analysis of elastic systems under nonconservative loading -Natural formulation. Part I.

Quasitatic problems,: *Comp. Meth. Appl. Mech. Engrg.* 26, 75-123

Argyris. J.H. and Sp. Symeonides, [1981], "A sequel to: Nonlinear finite element analysis of elastic systems under nonconservative loading -Natural formulation. Part I. Quasitatic problems,: *Comp. Meth. Appl. Mech. Engrg.* 26, 377-383

Argyris, J.H., [1982], "An excursion into large rotations," *Comp. Meth. Appl. Mech. Engn.*, 32, pp.85-155.

Arnold, V. I., [1980], *Mathematical Methods of Classical Mechanics*, Springer-Verlag, New York.

Bathe, K.J., and S. Bolourchi, [1979], "Large displacement analysis of three dimensional beam structures," *Int. J. Num. Meth. Engng.*, 14, 961-986.

Belytschko, T., H. Stolarski and N. Carpenter, [1984], "A triangular plate element with one-point quadrature," Comp. Meth. Appl. Mech. Engng., 15, 63-81.

Bufler, H. [1984], "Pressure loaded structures under large deformations," *ZAMM., Z. Angew. Math. u. Mech.*, 64, 7, 287-295, *Int. J. Num. Meth. Engrg.*, 20 787-802.

Ciarlet, P. G., [1978], *The Finite Element Method for Elliptic Problems* , North Holland Publishers Co.

Carey, J., and J.T. Oden, [1983], *Finite Element Vol II. Texas Series in Computational Mechanics*, Prentice Hall, Inc., N.J.

DaDeppo, D. A., and R. Schmidt, [1975], "Instability of Clamped-Hinged Circular Arches Subjected to a Point Load," *Trans. Am. Soc. Mech. Eng.*, ASME, Vol. 97 (3).

De Veubeke, B.F., [1976], "The dynamics of flexible bodies," *J. Eng. Science.*, 14, 895-913.

Hughes T. J. R., and J. Winget [1980], "Finite rotation effects in numerical integration of rate constitutive equations arising in large-deformation analysis," *Int. J. Num. Meth. Engng.* 15, No.9, pp.1413-1418

Hughes, T.J.R., [1984] "Numerical implementation of constitutive models: Rate independent deviatoric plasticity," in *Theoretical foundations for large scale computations*, S. Nemat-Nasser, R. Asaro and G. Hegemier Edts. Mechanics of elastic and inelastic solids 6, Martinus Nijhoff Publishers.

Hughes, T.J.R. and T.E. Tezduyar, [1981], "Finite elements based upon Mindlin plate theory with particular reference to the four node bilinear isoparametric element," *J. Appl. Mech* 48 587-596.

Kane, T.R., P.W. Likins, D.A. Levinson, [1983], *Spacecraft Dynamics*, McGraw-Hill Book Co., New York.

Love, A.E.H., [1944], *The mathematical theory of elasticity*, Dover Publications, New York.

Lowrie J.W., [1979], "Autonomous Attitude Determination Systems," in *Advances in The Astronautical Sciences* series, *Guidance and Control 1979*, , pp. 53-92, An American Astronautical Society Publication.

Malkus, D.S. and T.J.R. Hughes, [1978], "Mixed Finite Element Methods-Reduced and Selective Integration Techniques: A Unification of Concepts," *Comp. Meth. Appl. Mech. Engng.* 15, pp. 63-81.

Marsden J.E. and T.J.R Hughes [1983], *Mathematical foundations of elasticity*, Prentice-Hall Englewood Cliffs, N.J.

Naghdi, P.M., [1980], "Finite deformations of elastic rods and shells," *Proc. IUTAM Symposium on Finite Elasticity*, Lehigh University.

Noor, A.K., and J.M. Peters, [1981], "Mixed models and selective/reduced integration displacement models for nonlinear analysis of curved beams," *Int. J. Num. Meth. Engng.*, 17, 615-631.

Nordgren, R.P., [1974] "On Computation of the Motion of Elastic Rods," *Journal of Applied Mechanics*, pp. 777-780.

Reissner, E., [1972], "On a one-dimensional finite strain beam theory: The Plane Problem," *J. Appl. Math. Phys.* 23, pp.795-804.

Reissner, E., [1982], "Some remarks on the problem of column buckling," *Ingenieur-Archiv*, 52, pp.115-119, Springer.

Riks, E., [1972], "The application of Newton's method to the problem of elastic stability," *J. Appl. Mech.*, Vol. 39, pp. 1060-1066.

Shweizerhof, K. & E. Ramm, [1984], "Displacement dependent pressure loads in nonlinear finite element analysis," *Comp. Struct.*, 18.

Simo, J.C., K.H. Hjelmstad & R.L. Taylor, [1984], "Numerical formulations for the elasto-viscoplastic response of beams accounting for the effect of shear," *Comp. Meth. Appl. Mech. Engn.*, 42, pp.301-330.

Simo, J.C. [1985], "A finite strain beam formulation. Part I: The three dimensional dynamic problem," *Comp. Meth. Appl. Mech. Engrg.*, (In press)

Simo, J.C., P. Wriggers and R.L. Taylor, [1984], "A Perturbed Lagrangian Formulation for the Finite Element Solution of Contact Problems," *Comp. Meth. Appl. Mech. Engng.*,

Simo, J.C., R.L. Taylor and K.S. Pister, [1985], "Variational and projection methods for the volume constraint in finite deformation of elasto-plasticity," *Comp. Meth. Appl. Mech. Engrg.*, (to appear)

Simo, J.C., P. Wriggers, K. Shweizerhof, and R.L. Taylor, "Finite deformation post-buckling analysis involving inelasticity and contact constraints," *ASME Anual Winter Meeting*, New Orleans, Nov. [1984].

Spivak, M., [1978], *A comprehensive introduction to differential geometry, Volume One*," Publish or Perish, Inc, Berkely.

Spurrier, [1978], "Comment on 'Singularity-Free Extraction of a Quaternion from a Direction-Cosine Matrix,'" *Journal of Spacecraft*, Vol. 15, No. 4, p. 255, Jul-Aug.

Stolarski, H. and T. Belytschko, "On the equivalence of mode decomposition and mixed finite elements," *Comp. Meth. Appl. Mech. Engrg.* (submitted for publication). To appear.

Wempner, G.A., [1972], "Discrete approximations related to non-linear theories of solids," *Int. J. Solids Structures*, Vol. 7, pp. 1581-1599.

Ziegler, H., [1977], *Principles of structural stability*," Birkhauser, Basel, 2nd ed.

Zienkiewicz, O. C., [1977], *The Finite Element Method* , Third Edition, McGraw-Hill, New York.

APPENDIX I: Derivative of the exponential map

In this appendix we give the derivation of the formulae in section 5.2. for the derivative of the exponential map. Given a skew-symmetric tensor field $\Theta(S)$ and its axial vector $\vartheta(S)$ representing an incremental rotation field, i.e.,

$$\Theta(S) = \begin{bmatrix} 0 & -\vartheta_3 & \vartheta_2 \\ \vartheta_3 & 0 & -\vartheta_1 \\ -\vartheta_2 & \vartheta_1 & 0 \end{bmatrix}, \qquad \vartheta(S) = \begin{Bmatrix} \vartheta_1 \\ \vartheta_2 \\ \vartheta_3 \end{Bmatrix}, \tag{I.1}$$

a closed form expression for the exponential of $\Theta(S)$ is given by the formula

$$\exp[\Theta(S)] = \mathbf{I} + \frac{2}{1 + \|\bar{\vartheta}\|^2}(\bar{\Theta} + \bar{\Theta}^2), \tag{I.2}$$

where $\bar{\vartheta}(S)$ is given by

$$\mathbf{e} = \frac{\vartheta}{\|\vartheta\|}, \qquad \bar{\vartheta} = \tan(\|\vartheta\|/2)\,\mathbf{e}, \tag{I.3}$$

and $\Theta(S)$ is the skew-symmetric tensor field with axial vector $\bar{\vartheta}(S)$. By taking the derivative with respect to S we find

$$\frac{d}{dS}\exp[\Theta(S)] = \frac{2}{1 + \|\bar{\vartheta}\|^2}\left(\bar{\Theta}' + \bar{\Theta}'\bar{\Theta} + \bar{\Theta}\bar{\Theta}' - \frac{2\bar{\vartheta}\cdot\bar{\vartheta}'(\bar{\Theta} + \bar{\Theta}^2)}{1 + \|\bar{\vartheta}\|^2}\right) \tag{I.4}$$

Upon noting the identity

$$\bar{\Theta}^3 = -\|\bar{\vartheta}\|\bar{\Theta}, \tag{I.4}$$

a lengthy but straight forward manipulation yields the result

$$\left(\frac{d}{dS}\exp[\Theta(S)]\right)\exp[-\Theta(S)] = \frac{2}{1 + \|\bar{\vartheta}\|^2}(\bar{\Theta}' + \bar{\Theta}\bar{\Theta}' - \bar{\Theta}'\bar{\Theta} + \mathbf{A}) \tag{I.5}$$

where $\mathbf{A}$ is given by

$$\mathbf{A} \equiv -\bar{\vartheta}\cdot\bar{\vartheta}'(\bar{\Theta} - \bar{\Theta}^2) - \bar{\Theta}\bar{\Theta}'\bar{\Theta} + \bar{\Theta}\bar{\Theta}'\bar{\Theta}^2 \tag{I.6}$$

It remains to show that indeed $\mathbf{A} \equiv \mathbf{0}$. This follows at once from the identities

$$\bar{\Theta}\bar{\Theta}'\bar{\Theta} \equiv -(\bar{\vartheta}\cdot\bar{\vartheta}')\bar{\Theta}, \qquad \bar{\Theta}\bar{\Theta}'\bar{\Theta}^2 \equiv -(\bar{\vartheta}\cdot\bar{\vartheta}')\bar{\Theta}^2 \tag{I.7}$$

In addition, it is also noted that the axial vector β of $(d\exp[\Theta]/dS)\exp[-\Theta]$ is given by the expression

$$\beta = \frac{2}{1 + \|\bar{\vartheta}\|^2}[\bar{\vartheta}' + (\bar{\vartheta} \times \bar{\vartheta}')] \tag{I.8}$$

APPENDIX II: Configuration Update: Implementation.

In this appendix, we discuss in detail practical considerations concerning the implementation of the update procedure based on the use of quaternion parameters. Details pertaining to the configuration update are considered first. The update of the curvature will be examined subsequently.

II.1. Update of the configuration.

The update of the deformed centroidal line poses no difficulty, and is summarized in Box 4. In what follows, we are concerned specifically with the update of the section rotation. To avoid the singularity at $\|\vartheta\| = (2n + 1)\pi$ in the formula

for the exponential map (see (*) in Box 4), use is made of the four quaternion parameters. This furnishes the optimal parametrization of three-dimensional rotations that avoids singularities. Recall that quaternions are elements of the hypercomplex space expressed as

$$\mathbf{q} = q_0 + \hat{\mathbf{q}}; \quad \hat{\mathbf{q}} = q_1\mathbf{e}_1 + q_2\mathbf{e}_2 + q_3\mathbf{e}_3 \tag{II.1}$$

where q_0 represents the scalar part, and $\hat{\mathbf{q}}$ the vector part of $\mathbf{q}$. For a unit quaternion, we have $\sum_{i=0}^{3} q_i^2 = 1$. In the above, we identify the spatial basis $(\mathbf{e}_1, \mathbf{e}_2, \mathbf{e}_3)$ with the imaginary basis of the hypercomplex space. Recall also the 1-1 correspondence between quaternions and orthogonal matrices. Hence, quaternion parameters are kept in the data base to minimize storage requirements. The update procedure may be summarized in the box below

BOX *II.* 1. *Update of quaternion describing section rotation.*

(i) Retrieve $\mathbf{q}_n$, and compute $\mathbf{\Lambda}_n$ from $\mathbf{q}_n$.
(ii) Compute $\mathbf{q}$ associated with $\boldsymbol{\vartheta}$.
(iii) Compute $\exp[\boldsymbol{\Theta}]$ from $\mathbf{q}$.
(iv) Perform $\mathbf{\Lambda}_{n+1} = \exp[\boldsymbol{\Theta}]\,\mathbf{\Lambda}_n$.
(v) Extract $\mathbf{q}_{n+1}$ from $\mathbf{\Lambda}_{n+1}$, and store $\mathbf{q}_{n+1}$.

The unit quaternion corresponding to an incremental rotation vector $\boldsymbol{\vartheta} \equiv \vartheta_1\mathbf{e}_1 + \vartheta_2\mathbf{e}_2 + \vartheta_3\mathbf{e}_3$ (see step (ii) in Box *II.* 1) is given by

$$\mathbf{q} = \cos\frac{\|\boldsymbol{\vartheta}\|}{2} + \frac{\boldsymbol{\vartheta}}{\|\boldsymbol{\vartheta}\|}\sin\frac{\|\boldsymbol{\vartheta}\|}{2} \tag{II.2}$$

The pseudo-vector of rotation $\bar{\boldsymbol{\vartheta}}$ is then the vector part of a unit quaternion whose scalar part is normalized to one:

$$\frac{\mathbf{q}}{q_0} = 1 + \frac{\hat{\mathbf{q}}}{q_0} = 1 + \bar{\boldsymbol{\vartheta}} \tag{II.3}$$

Clearly, singularity occurs when $\|\bar{\boldsymbol{\vartheta}}\| = (2n+1)\pi$, i.e., when $q_0 \equiv \cos(\|\bar{\boldsymbol{\vartheta}}\|/2) = 0$.

An orthogonal matrix $\mathbf{Q}$ is computed from its associated unit quaternion $\mathbf{q}$ by means of the relation

$$\mathbf{Q} = 2\begin{bmatrix} q_0^2 + q_1^2 - \tfrac{1}{2} & q_1q_2 - q_3q_0 & q_1q_3 + q_2q_0 \\ q_2q_1 + q_3q_0 & q_0^2 + q_2^2 - \tfrac{1}{2} & q_2q_3 - q_1q_0 \\ q_3q_1 - q_2q_0 & q_3q_2 + q_1q_0 & q_0^2 + q_3^2 - \tfrac{1}{2} \end{bmatrix} \tag{II.4}$$

This applies to steps (i) and (iii) in Box *II.* 1.

Given an orthogonal matrix $\mathbf{Q}$, the associated quaternion parameters can be obtained from (II.4) by

$$\begin{aligned} q_0 &= \pm\tfrac{1}{2}\sqrt{1 + \mathrm{Tr}(\mathbf{Q})} \\ q_1 &= \pm(Q_{32} - Q_{23})/4q_0 \\ q_2 &= \pm(Q_{13} - Q_{31})/4q_0 \\ q_3 &= \pm(Q_{21} - Q_{12})/4q_0 \end{aligned} \tag{II.5}$$

where $\mathrm{Tr}(\mathbf{Q}) = Q_{ii}$. Note that we only need to determine the sign of q_0, as the sign of q_1, q_2, q_3 will follow. Either a positive or negative sign for q_0 is possible; to fix the choice, we may choose $q_0 \geq 0$. However, relations (II.5) suffer from round-off errors since the numerators and the denominators in q_1, q_2, q_3 are obtained from subtraction of nearly equal quantities in the vicinity of 0^0 and 180^0. Moreover, the computation breaks down when the rotation is exactly 180^0, e.g., as in the case of $\mathbf{Q} = Diag(-1,-1,1)$. There are several proposed algorithms to extract a quaternion from an orthogonal transformation matrix. Among them, the algorithm proposed by Spurrier [1978] was reported to be the fastest (Lowrie [1979]), and is summarized in Box *II.2*.

BOX *II.2. Spurrier's algorithm for quaternion extraction.*

$M \triangleq \max(\mathrm{Tr}(\mathbf{Q}); Q_{11}, Q_{22}, Q_{33})$

If $M = \mathrm{Tr}(\mathbf{Q})$, then:

$$q_0 = \tfrac{1}{2}\sqrt{1 + \mathrm{Tr}(\mathbf{Q})}$$

$$q_i = (Q_{kj} - Q_{jk})/4q_0, \quad \text{for } i=1,2,3$$

Else:

Let i be such that $M = Q_{(ii)}$,

$$q_i = \left[\frac{Q_{(ii)}}{2} + \frac{1 - \mathrm{Tr}(\mathbf{Q})}{4}\right]^{1/2}$$

$$q_0 = (Q_{kj} - Q_{jk})/4q_i$$

$$q_l = (Q_{li} + Q_{il})/4q_i, \quad \text{for } l=j,k$$

where i,j,k is a cyclic permutation of 1,2,3.

II.2. Update of the spatial curvature vector.

The skew-symmetric matrix $\boldsymbol{\Omega}$ associated with the spatial curvature vector $\boldsymbol{\omega}$ is updated according to

$$\boldsymbol{\Omega}_{n+1} = \frac{d\exp[\boldsymbol{\Theta}]}{dS}\exp[-\boldsymbol{\Theta}] + \exp[\boldsymbol{\Theta}]\,\boldsymbol{\Omega}_n \exp[-\boldsymbol{\Theta}] \tag{II.6}$$

In the actual implementation, direct update of the axial vector $\boldsymbol{\omega}$ is obtained in two steps:

(i) Compute the axial vector associated with the second term $(\exp[\boldsymbol{\Theta}]\,\boldsymbol{\Omega}_n \exp[-\boldsymbol{\Theta}])$ in (II.6).

(ii) Evaluate the axial vector $\boldsymbol{\beta}$ of the term $\left(\frac{d\exp[\boldsymbol{\Theta}]}{dS}\right)\exp[-\boldsymbol{\Theta}]$ by

$$\boldsymbol{\beta} = \frac{\sin\|\boldsymbol{\vartheta}\|}{\|\boldsymbol{\vartheta}\|}\boldsymbol{\vartheta}' + \left[1 - \frac{\sin\|\boldsymbol{\vartheta}\|}{\|\boldsymbol{\vartheta}\|}\right]\left(\frac{\boldsymbol{\vartheta}\cdot\boldsymbol{\vartheta}'}{\|\boldsymbol{\vartheta}\|}\right)\frac{\boldsymbol{\vartheta}}{\|\boldsymbol{\vartheta}\|} + \tfrac{1}{2}\left[\frac{\sin\|\boldsymbol{\vartheta}\|/2}{\|\boldsymbol{\vartheta}\|/2}\right]^2 \boldsymbol{\vartheta}\times\boldsymbol{\vartheta}' \tag{II.7}$$

obtained from (I.8) in Appendix I and from the expressions of $\overline{\boldsymbol{\vartheta}}$ and $\overline{\boldsymbol{\vartheta}}'$ in Box 4. The sum of the above two axial vectors then yields the updated spatial curvature vector. We observe that $\boldsymbol{\beta} \approx \boldsymbol{\vartheta}'$ for $\|\boldsymbol{\vartheta}\|$ small, i.e., $\boldsymbol{\vartheta}'$ is a first approximation of $\boldsymbol{\beta}$ as was noted in Remark 5.1.

Figure Captions

Fig. 2.1. Kinematic description of the rod for the plane problem. Definition of various frames.

Fig. 3.1. Geometric interpretation of the exponential map.

Fig. 7.1. Pure bending of a cantilever beam subject to end moment. *One* load step. *Two* iterations to convergence.

Fig. 7.2.a. Cantilever beam subject to follower end load. Deformed shapes.

Fig. 7.2.b. Cantilever beam subject to follower end load. Vertical and horizontal tip displacement vs. applied end load.

Fig. 7.3.a. Clamped-hinged deep circular arch subject to point load. Deformed shapes.

Fig. 7.3.b. Clamped-hinged deep circular arch subject to point load. Applied load vs. vertical and horizontal displacements of the apex.

Fig. 7.4.a. Snap-through of a hinged right-angle frame under fixed point load. Deformed shapes.

Fig. 7.4.b. Snap-through of a hinged right-angle frame under follower point load. Deformed shapes.

Fig. 7.4.c. Snap-through of a hinged right-angle frame under fixed and follower load. Load vs. vertical displacement under applied load.

Fig. 7.4.d. Snap-through of a hinged right-angle frame under fixed and follower load. Load vs. horizontal displacement under applied load.

Fig. 7.5.a. Cantilever 45*degree* bend subject to fixed end load. Perspective view of deformed shapes.

Fig. 7.5.b. Cantilever 45*degree* bend subject to fixed end load. Projection of deformed shapes onto the x-y plane.

Fig. 7.5.c. Cantilever 45*degree* bend subject to fixed end load. Components of tip displacement vs. applied load.

Fig. 7.5.d. Cantilever 45*degree* bend subject to follower end load. Perspective view of deformed shapes.

Fig. 7.5.e. Cantilever 45*degree* bend subject to follower end load. Projection of deformed shapes onto the x-y plane.

Fig. 7.5.f. Cantilever 45*degree* bend subject to follower end load. Components of tip displacement vs. applied load.

Fig. 7.6.a. Lateral buckling of a cantilever right-angle frame under end load. Geometry and perspective view of final deformed shape.

Fig. 7.6.b. Lateral buckling of a cantilever right-angle frame under end load. Projection of final deformed shape onto the x-z plane.

Fig. 7.6.c. Lateral buckling of a cantilever right-angle frame under end load. Applied load vs. lateral tip displacement of the free end.

Fig. 7.7.a. Lateral buckling of a hinged right-angle frame subject to fixed end moment. Geometric characteristics.

Fig. 7.7.b. Lateral buckling of a hinged right-angle frame subject to fixed end moment. First revolution: perspective view of deformed shapes at various load level.

Fig. 7.7.c. Lateral buckling of a hinged right-angle frame subject to fixed end moment. First revolution: projection of deformed shapes onto the y-z plane.

Fig. 7.7.d. Lateral buckling of a hinged right-angle frame subject to fixed end moment. First revolution: applied end moment vs. abscissa of left hinged end.

Fig. 7.7.e. Lateral buckling of a hinged right-angle frame subject to fixed end moment. First and second revolution: applied end moment vs. lateral displacement of the apex.

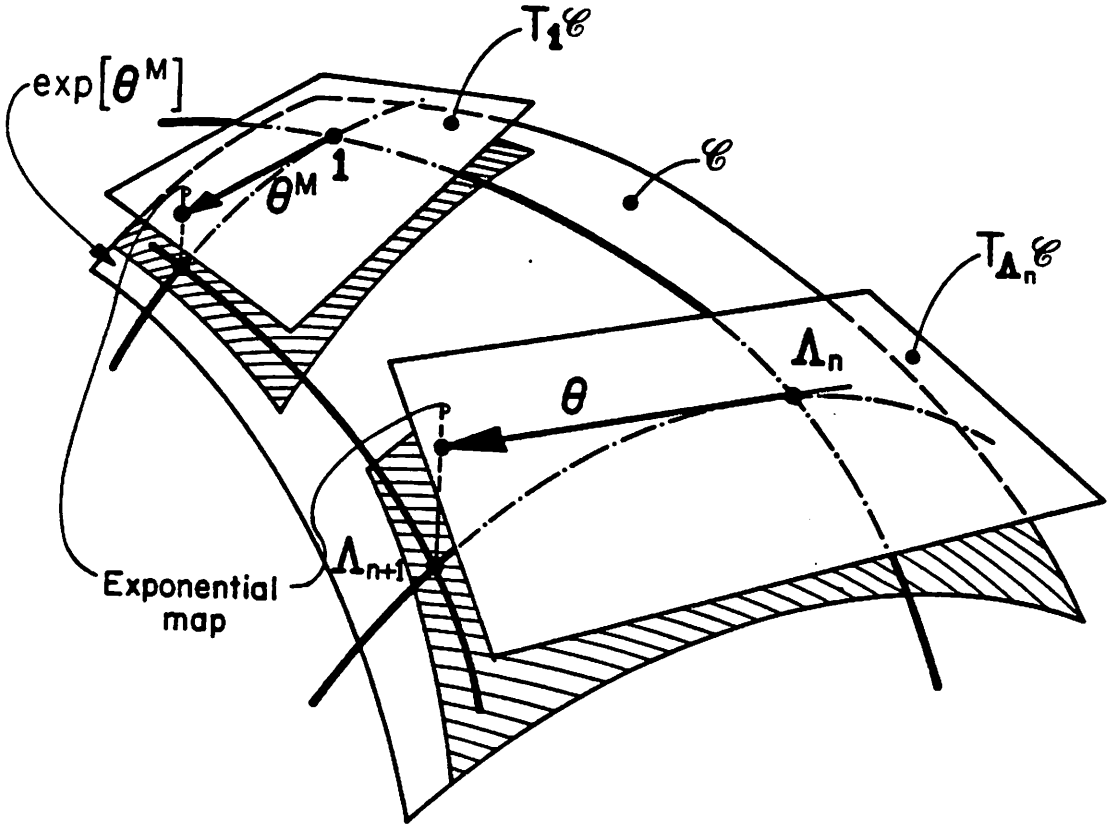

Fig. 3.1. Geometric interpretation of the exponential map.

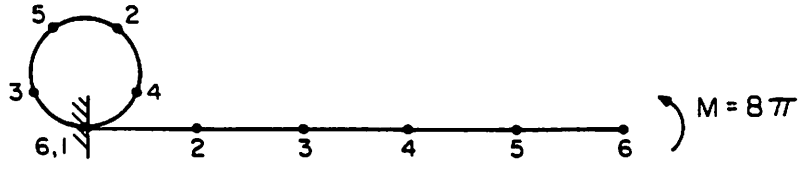

Fig. 7.1. Pure bending of a cantilever beam subject to end moment. *One* load step. *Two* iterations to convergence.

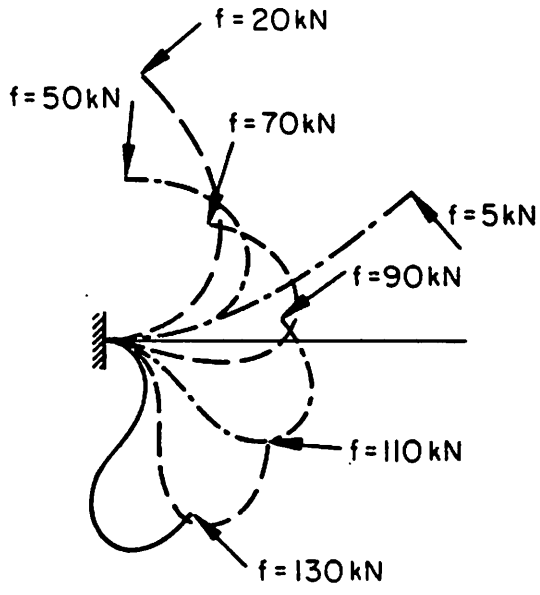

Fig. 7.2.a. Cantilever beam subject to follower end load. Deformed shapes.

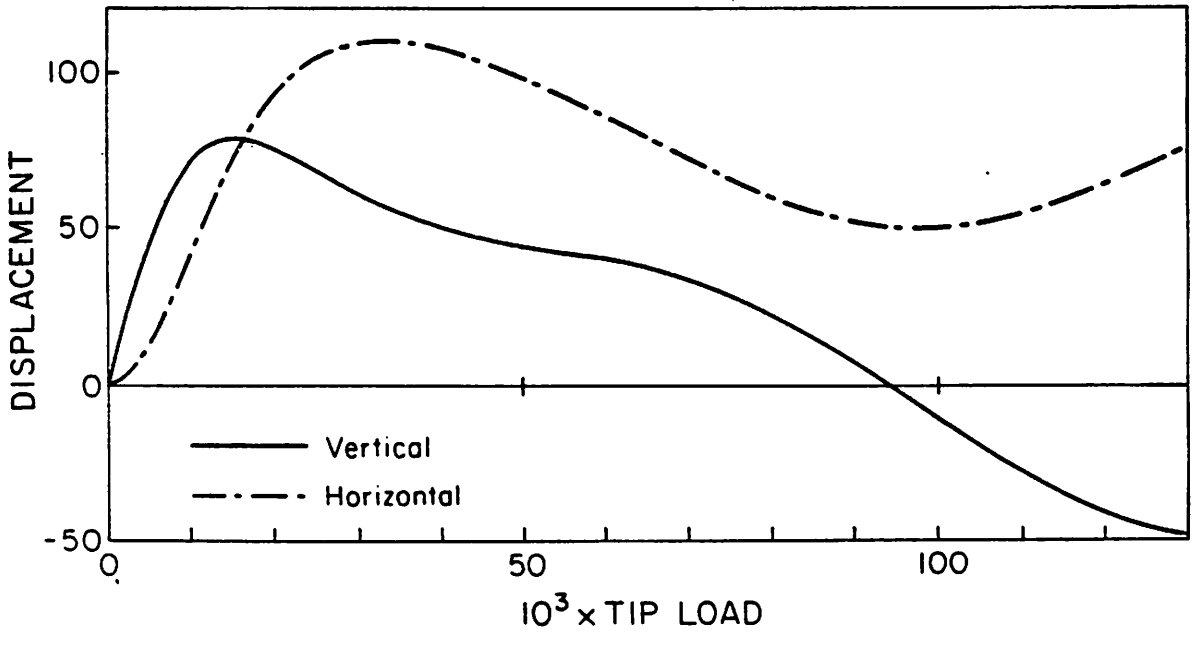

Fig. 7.2.b. Cantilever beam subject to follower end load. Vertical and horizontal tip displacement vs. applied end load.

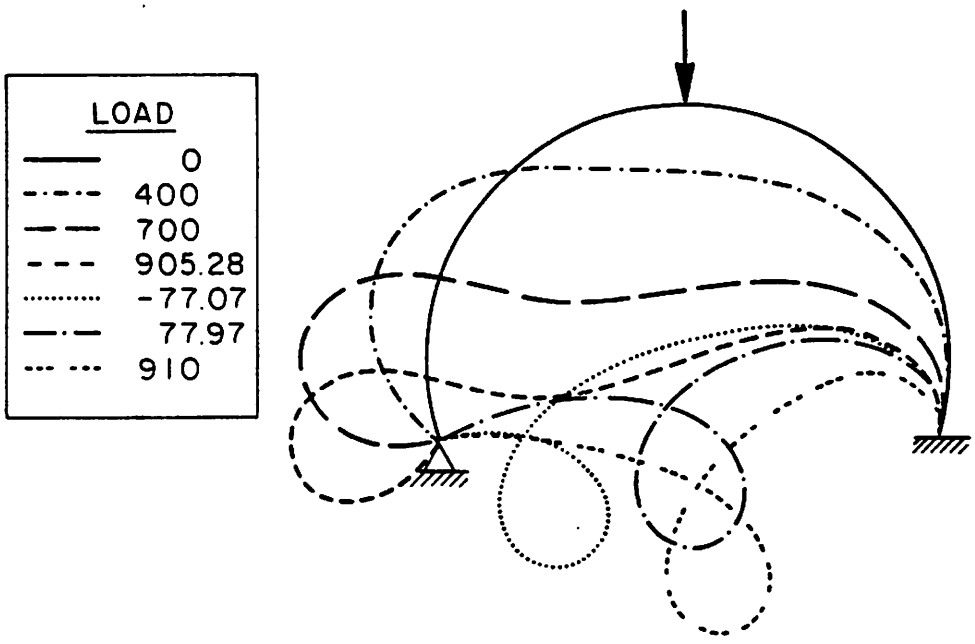

Fig. 7.3.a. Clamped-hinged deep circular arch subject to point load. Deformed shapes.

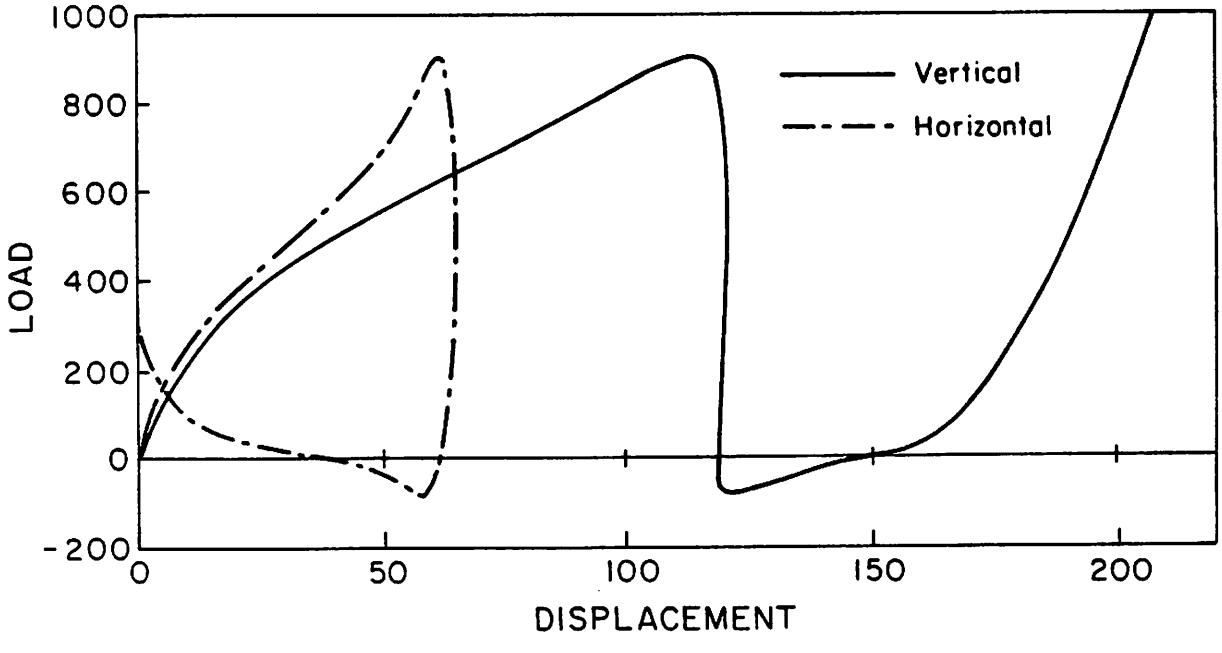

Fig. 7.3.b. Clamped-hinged deep circular arch subject to point load. Applied load vs. vertical and horizontal displacements of the apex.

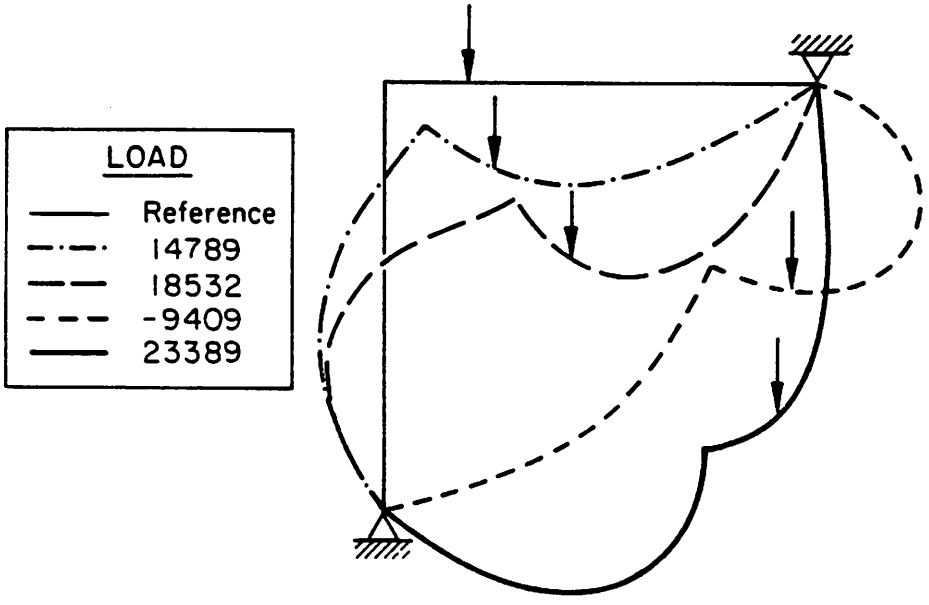

Fig. 7.4.a. Snap-through of a hinged right-angle frame under fixed point load. Deformed shapes.

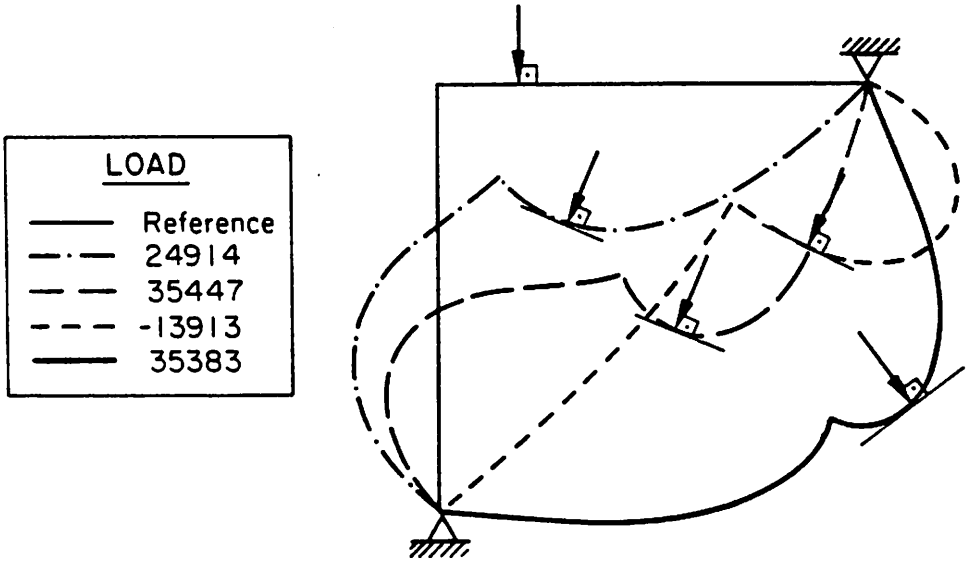

Fig. 7.4.b. Snap-through of a hinged right-angle frame under follower point load. Deformed shapes.

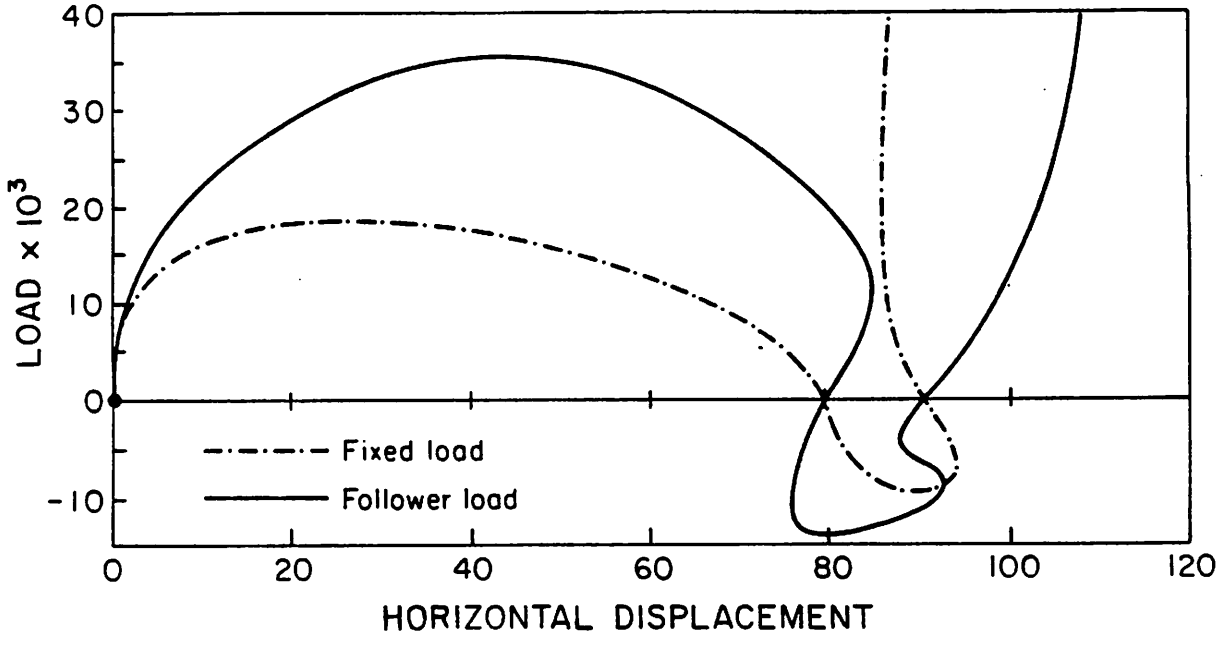

Fig. 7.4.d. Snap-through of a hinged right-angle frame under fixed and follower load. Load vs. horizontal displacement under applied load.

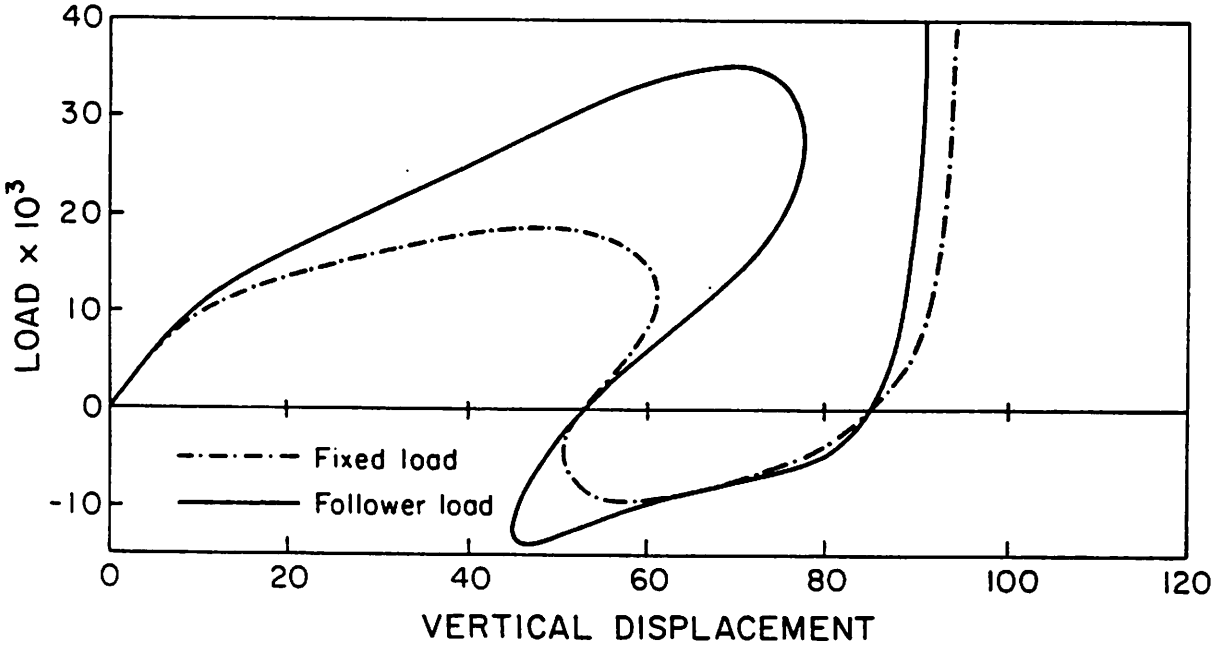

Fig. 7.4.c. Snap-through of a hinged right-angle frame under fixed and follower load. Load vs. vertical displacement under applied load.

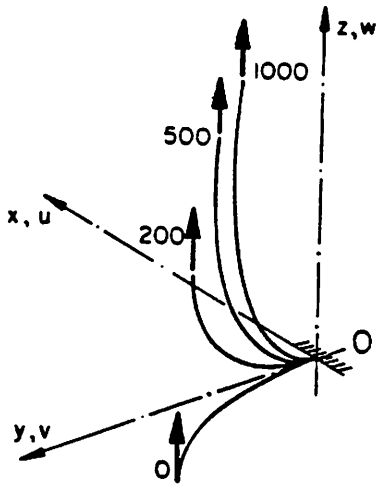

Fig. 7.5.a. Cantilever 45*degree* bend subject to fixed end load. Perspective view of deformed shapes.

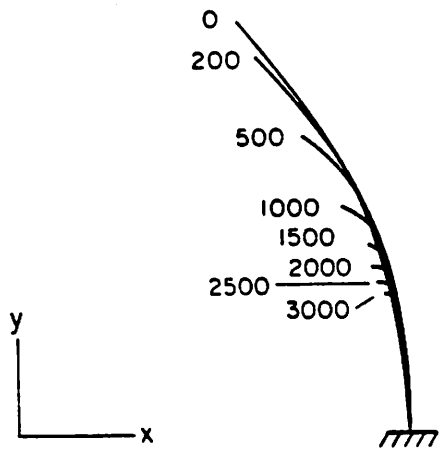

Fig. 7.5.b. Cantilever 45*degree* bend subject to fixed end load. Projection of deformed shapes onto the x-y plane.

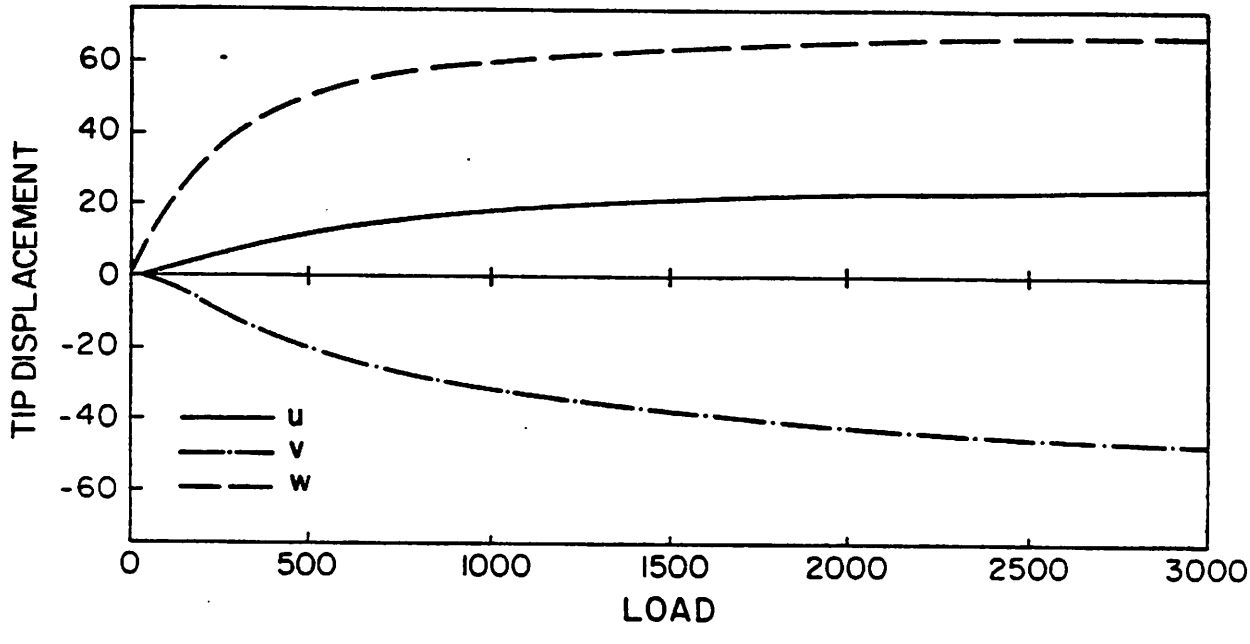

Fig. 7.5.c. Cantilever 45*degree* bend subject to fixed end load. Components of tip displacement vs. applied load.

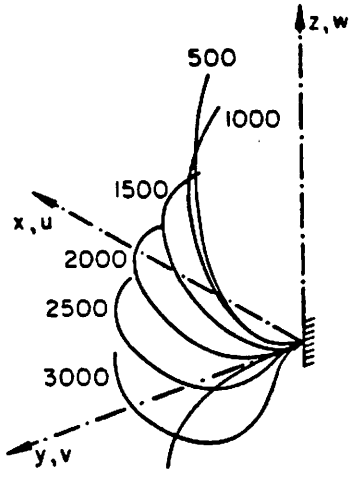

Fig. 7.5.d. Cantilever 45*degree* bend subject to follower end load. Perspective view of deformed shapes.

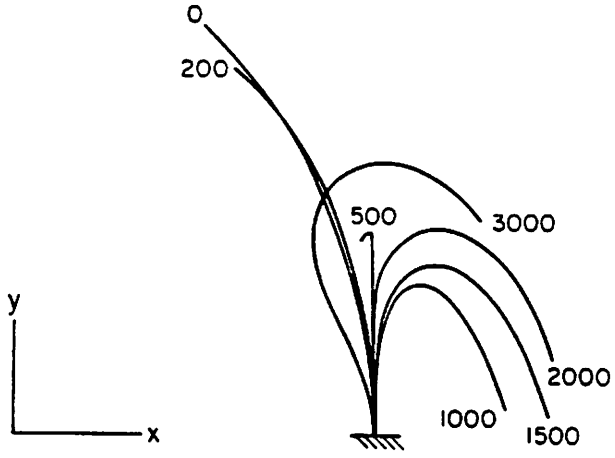

Fig. 7.5.e. Cantilever 45*degree* bend subject to follower end load. Projection of deformed shapes onto the x-y plane.

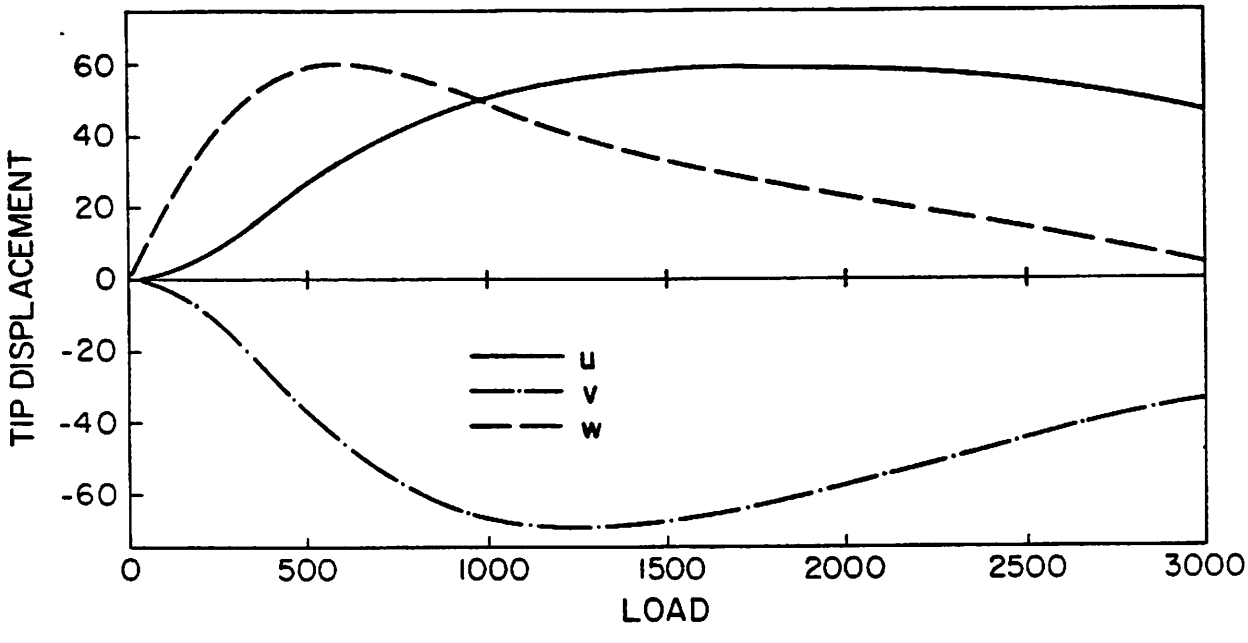

Fig. 7.5.f. Cantilever 45*degree* bend subject to follower end load. Components of tip displacement vs. applied load.

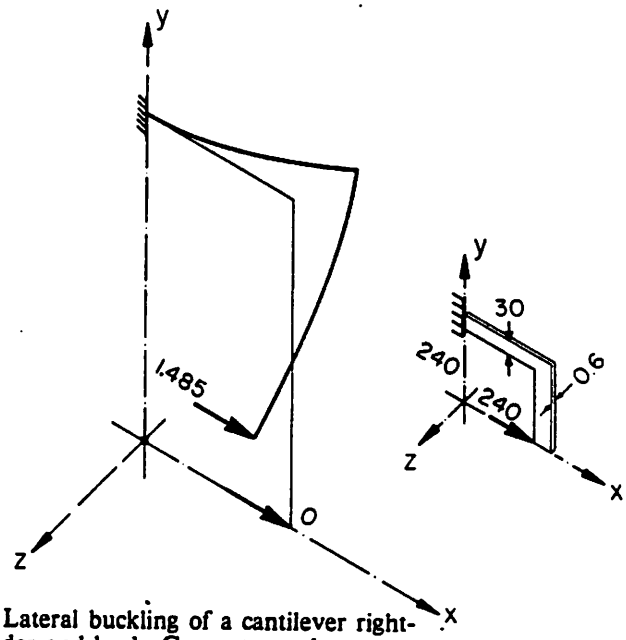

Fig. 7.6.a. Lateral buckling of a cantilever right-angle frame under end load. Geometry and perspective view of final deformed shape.

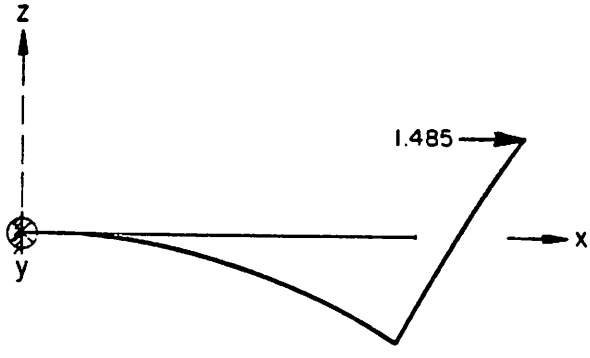

Fig. 7.6.b. Lateral buckling of a cantilever right-angle frame under end load. Projection of final deformed shape onto the x-z plane.

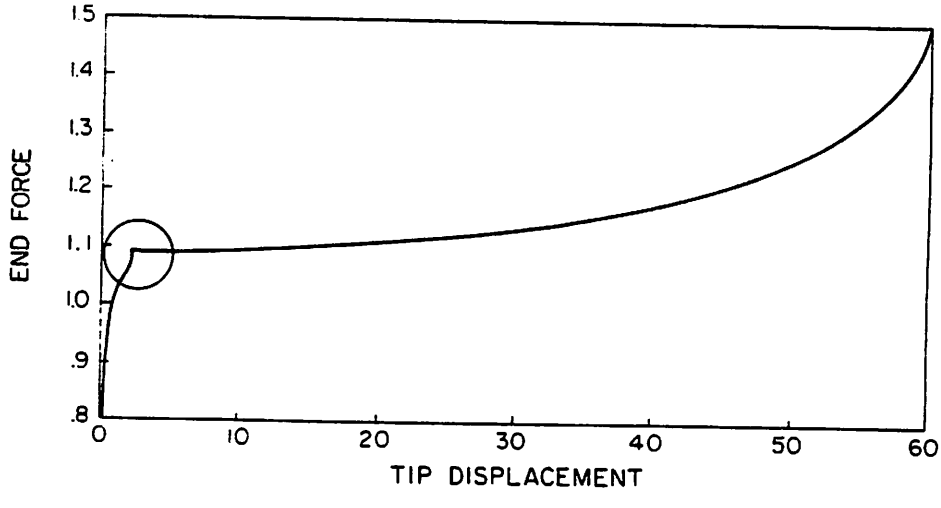

Fig. 7.6.c. Lateral buckling of a cantilever right-angle frame under end load. Applied load vs. lateral tip displacement of the free end.

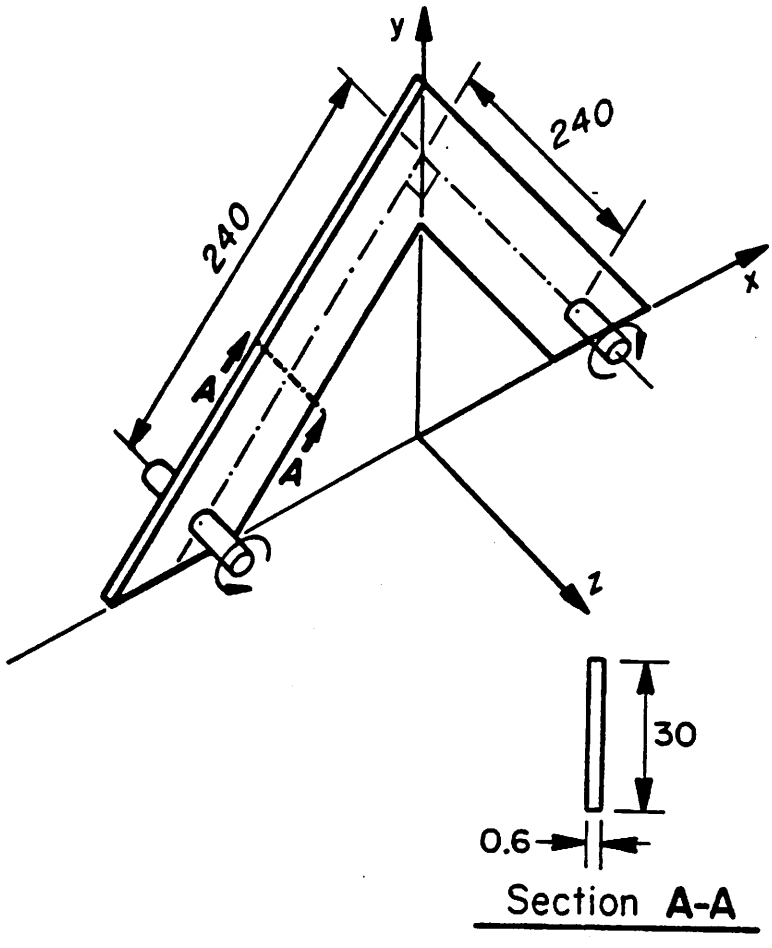

Fig. 7.7.a. Lateral buckling of a hinged right-angle frame subject to fixed end moment. Geometric characteristics.

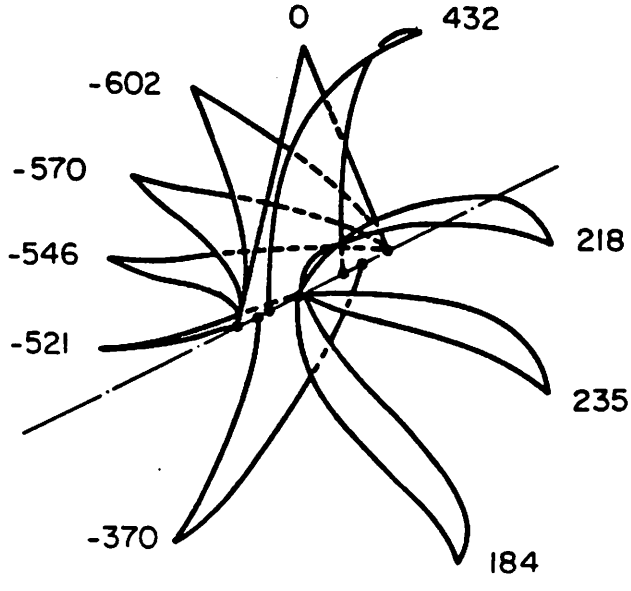

Fig. 7.7.b. Lateral buckling of a hinged right-angle frame subject to fixed end moment. First revolution: perspective view of deformed shapes at various load level.

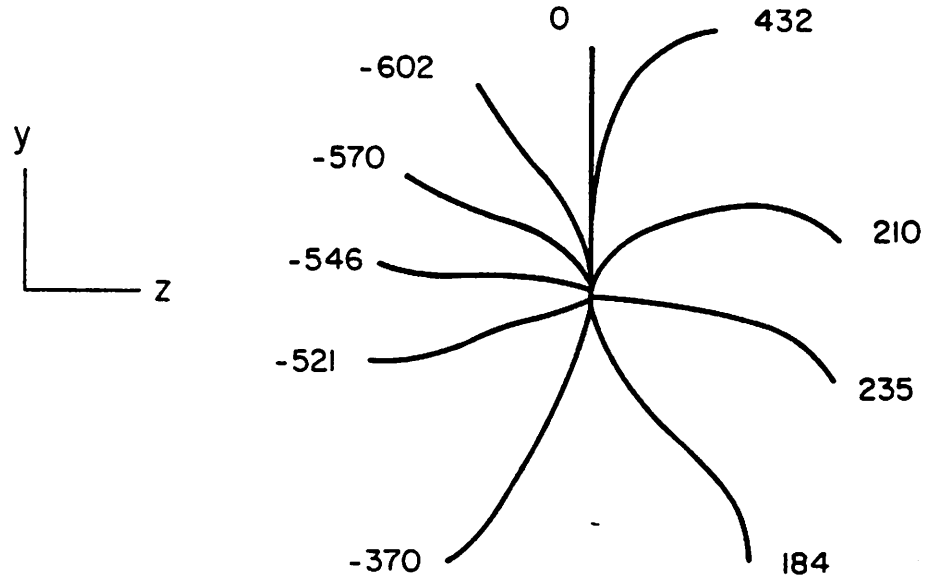

Fig. 7.7.c. Lateral buckling of a hinged right-angle frame subject to fixed end moment. First revolution: projection of deformed shapes onto the y-z plane.

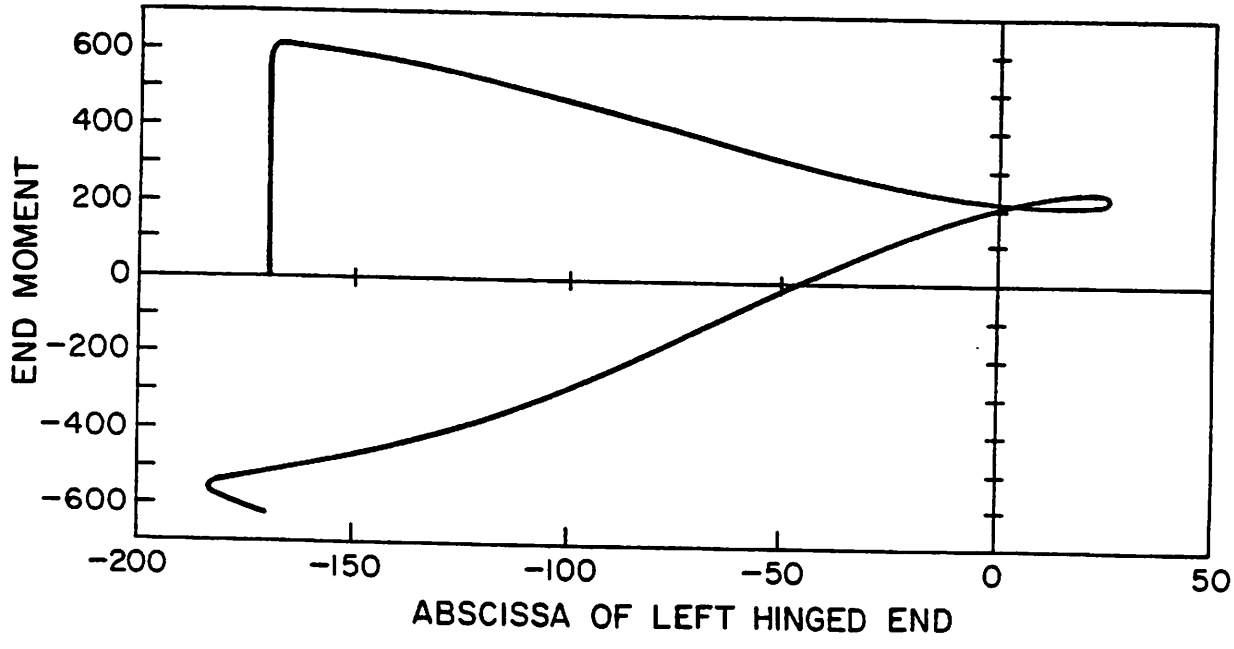

Fig. 7.7.d. Lateral buckling of a hinged right-angle frame subject to fixed end moment. First revolution: applied end moment vs. abscissa of left hinged end.

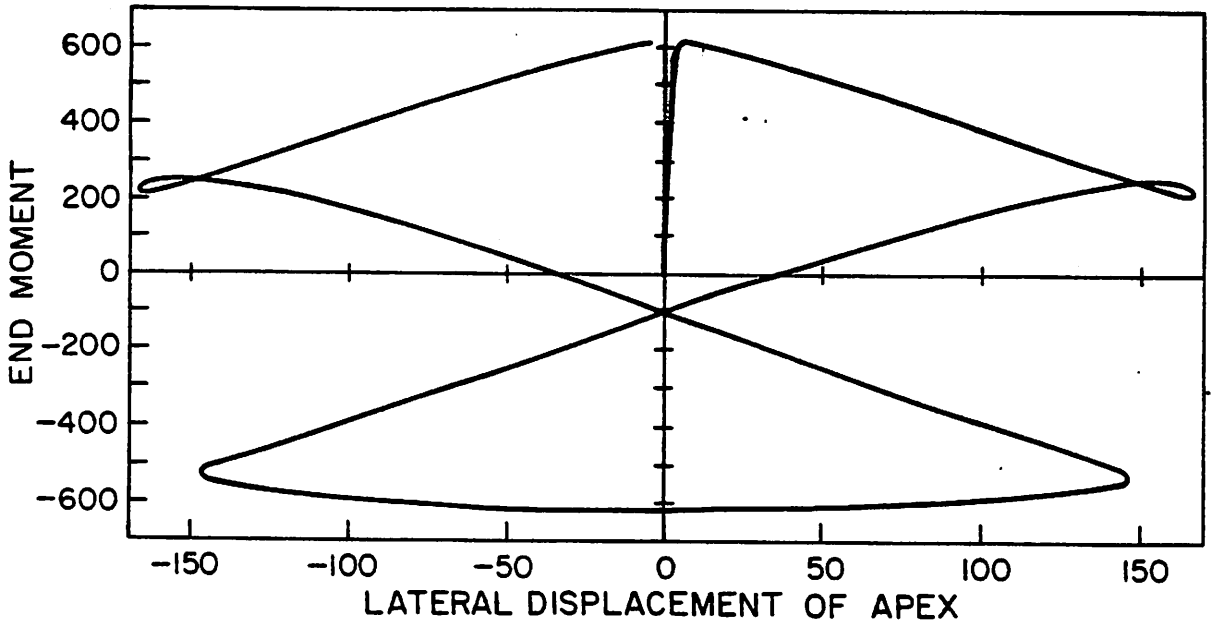

Fig. 7.7.e. Lateral buckling of a hinged right-angle frame subject to fixed end moment. First and second revolution: applied end moment vs. lateral displacement of the apex.